Supporting Information for Publication

Theoretical assessments of Pd-PdO phase transformation and its impacts on H_2O_2 synthesis and decomposition pathways

Manasi Vyas, Fernando Fajardo-Rojas, Diego A Gómez-Gualdrón, Stephanie Kwon*
Department of Chemical and Biological Engineering, Colorado School of Mines,
Golden, Colorado 80401, United States

* *Corresponding author: kwon@mines.edu*

S1. Molecular dynamic (MD) simulations for Pd_{13}, Pd_{55} and PdO clusters.

Figure S1 describes the methodology used for finding low energy cluster configurations for Pd_{13}, $Pd_{55,}$ and $Pd_{13}O_y$ clusters. This technique uses both Density Functional Theory (DFT) and reactive force-field Molecular Dynamics (ReaxFF MD) in an iterative DFT/MD/DFT process. For Pd clusters, following lattice parameter optimization for bulk Pd, clusters were constructed from the bulk based on a set number of Pd atoms (i.e. 13 and 55 atoms for Pd_{13} and Pd_{55}, respectively) as outlined in previous studies.[1–4] These clusters were optimized using DFT and were then used as initial configurations for ReaxFF MD annealing runs. For each run, ReaxFF took the initial DFT-derived cluster configurations and relaxed all atoms under the NVT ensemble using the Nose-Hoover thermostat. Each cluster was subject to two heating and cooling stages. The heating stages involved an increase in temperature to 400 K and a further increase to 1200 K with equilibrium stages between each step. The cooling stages followed the same methodology, with a decrease in temperature from 1200 K to 400 K and 400 K to 200 K. This procedure allowed the system to screen through different cluster configurations during the time frame of the simulation. Alternatively, the Berendsen thermostat was used with a 25 fs damping parameter and the PdxOy cluster was allowed to sample configurations during a single 0.750 ns stage of equilibration at 700 K. In all cases, the lowest energy cluster configurations found through ReaxFF were then re-optimized using DFT and compared with the initial DFT-derived cluster configuration guesses. Finally, the lowest energy clusters found by comparing the values from both DFT and ReaxFF were used for further H_2O_2 synthesis/decomposition DFT calculations.

Two methodologies were used to construct bulk $Pd_{13}O_y$ clusters. In the first method, we sequentially added O-atoms on the optimized Pd_{13} cluster and optimized each cluster via iterative DFT/MD/DFT simulations at each coverage (using the annealing method described above). In the second method, $Pd_{13}O_y$ clusters (y = 6-16) were cleaved from bulk PdO (after lattice optimization), which was further optimized via constant temperature DFT-MD-DFT iterations (at 700 K). These clusters were compared with those found from method 1, and the lowest energy $Pd_{13}O_y$ cluster was further used for H_2O_2 synthesis/decomposition calculations.

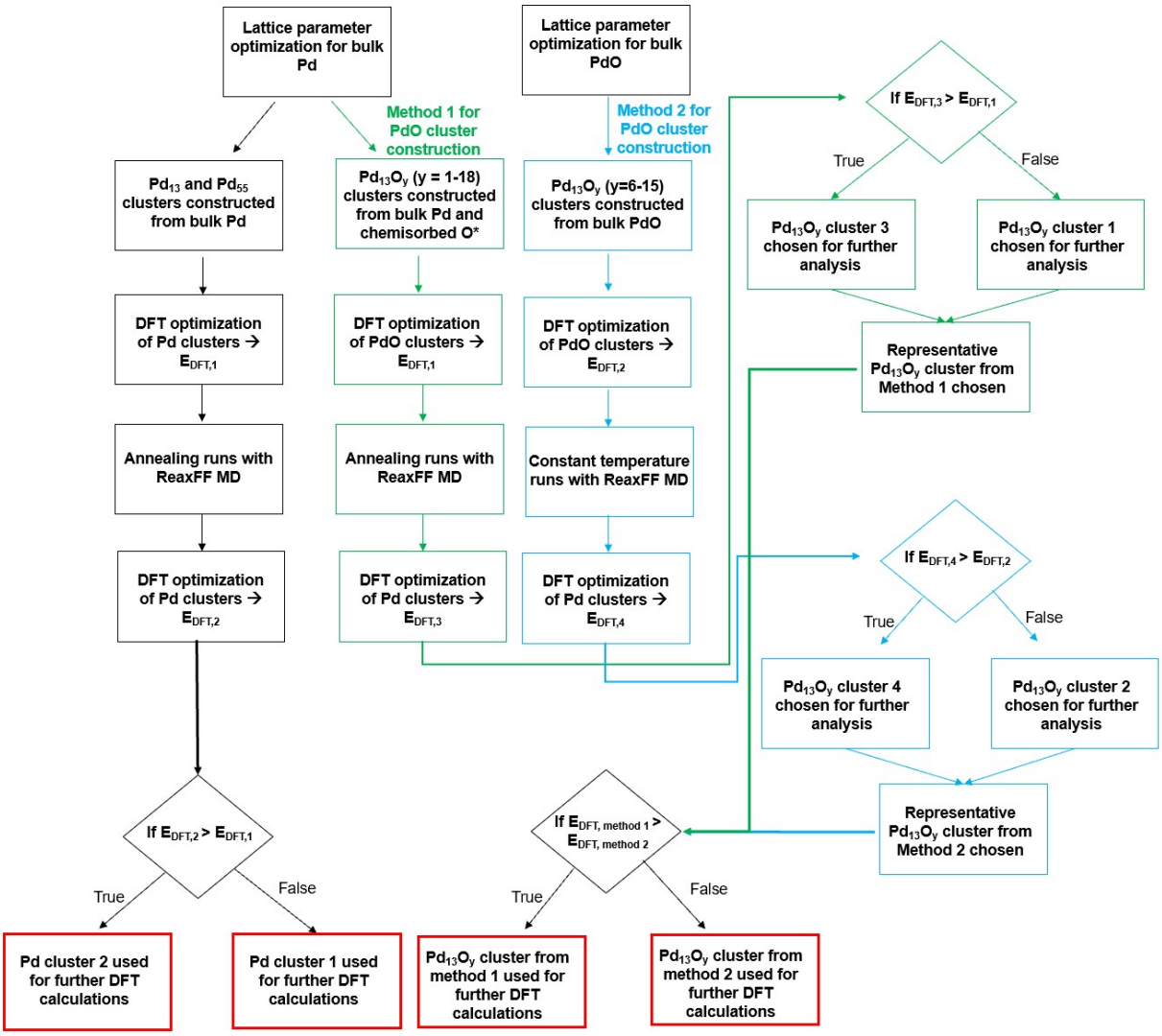

Figure S1. Iterative DFT/MD/DFT methodology used to find the lowest energy configurations of Pd and PdO clusters.

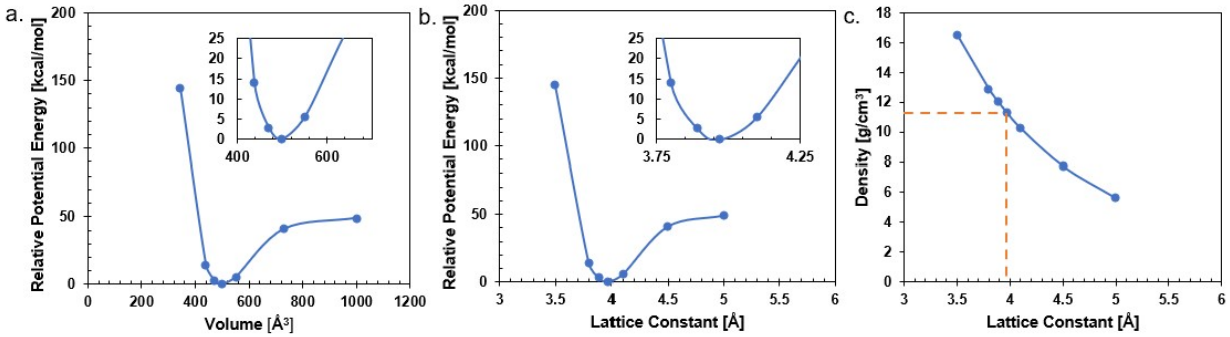

Figure S2. a) Birch-Murnaghan equation of state fit to the minima of the ReaxFF bulk Pd curve. b) ReaxFF expansion-compression curve for bulk Pd lattice parameter optimization. c) Density fitting for bulk Pd using ReaxFF derived lattice parameter.

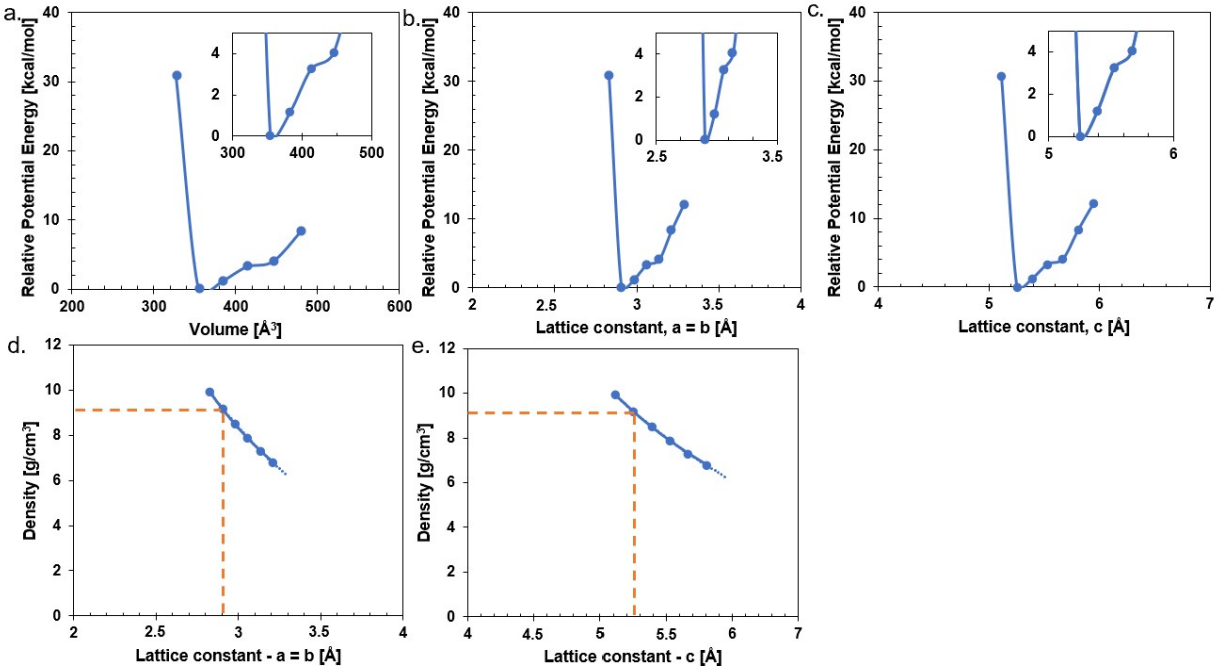

Figure S3. a) Birch-Murnaghan equation of state fit to the minima of the ReaxFF bulk PdO curve. b,c) ReaxFF expansion-compression curve for bulk PdO lattice parameter optimization. d,e) Density fitting for bulk PdO using ReaxFF derived lattice parameters.

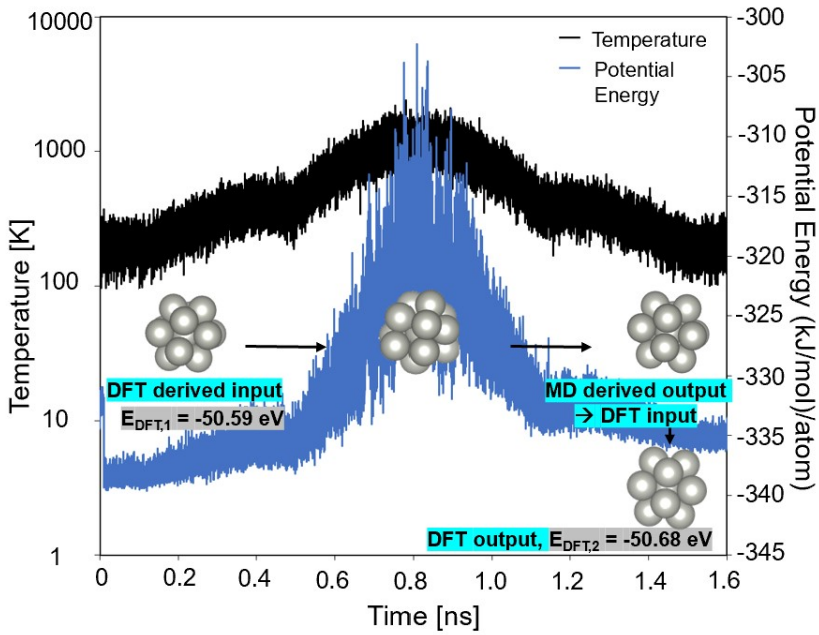

Figure S4. A DFT/MD/DFT run with ReaxFF annealing calculation for Pd_{13}, where temperature is the black curve and potential energy is the blue curve.

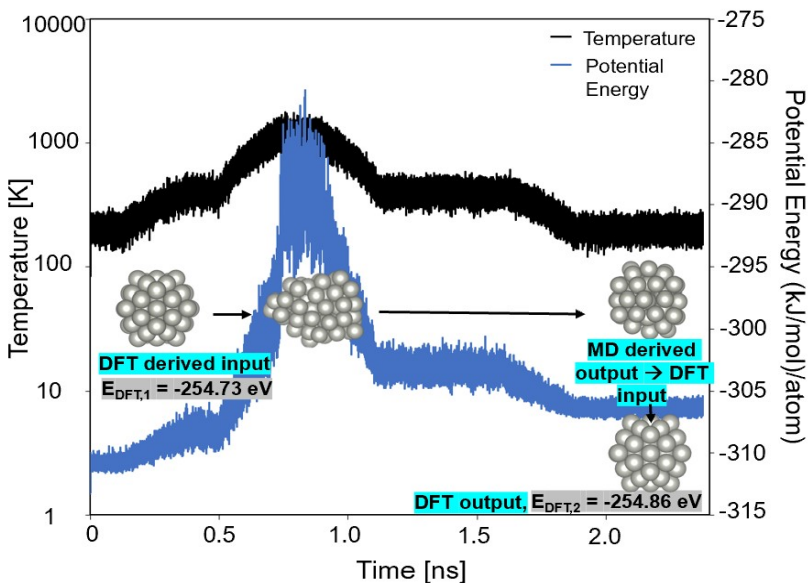

Figure S5. A DFT/MD/DFT run with ReaxFF annealing calculation for Pd_{55}, where temperature is the black curve and potential energy is the blue curve.

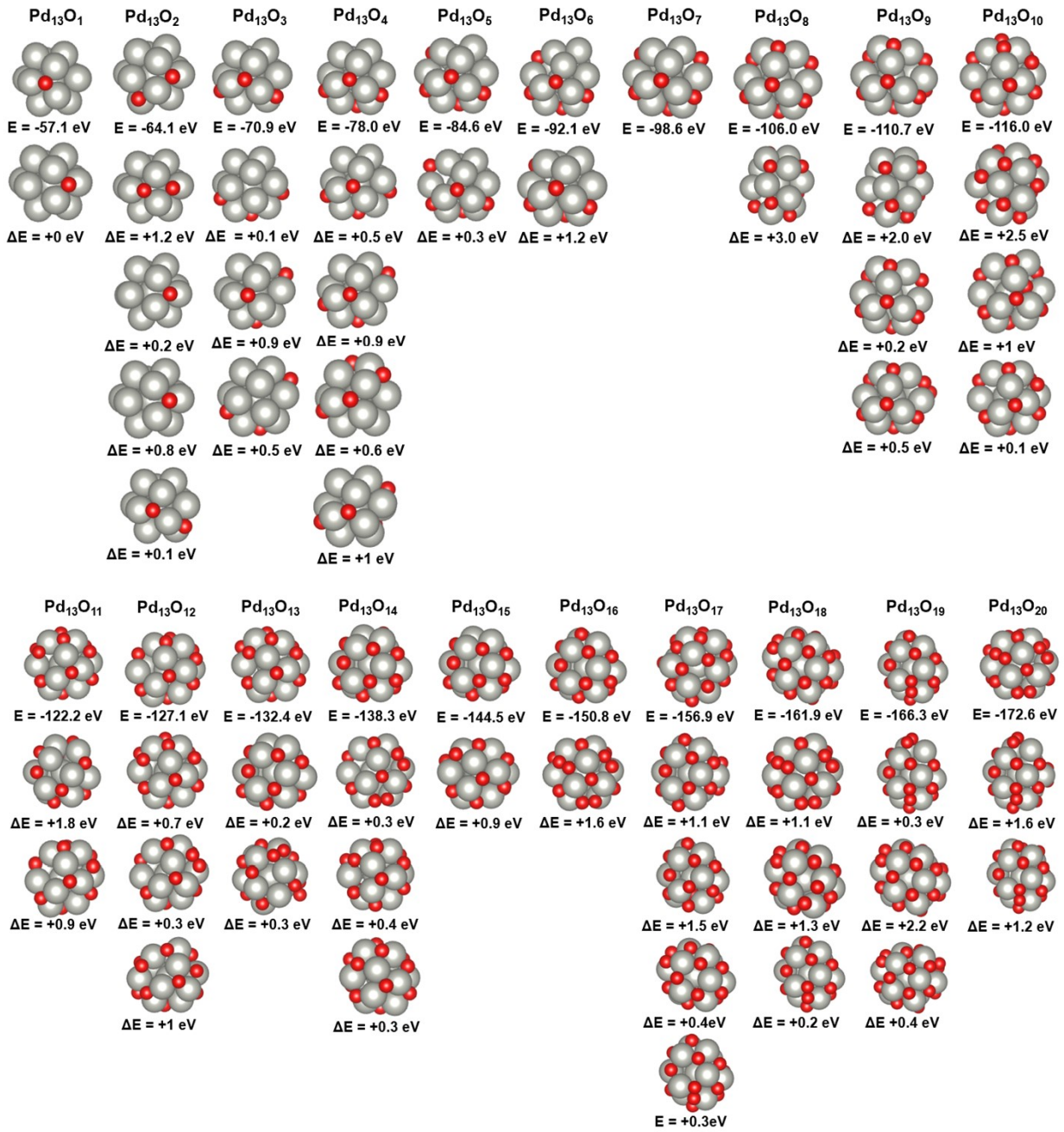

Figure S6. Comparison of DFT-derived electronic energies for Pd_{13} clusters with O* coverages ranging from 1-20 O* atoms and different configurations for each surface coverage. These clusters are used for further MD-DFT optimization (method 1) in PdO cluster construction, as outlined in S1.1.

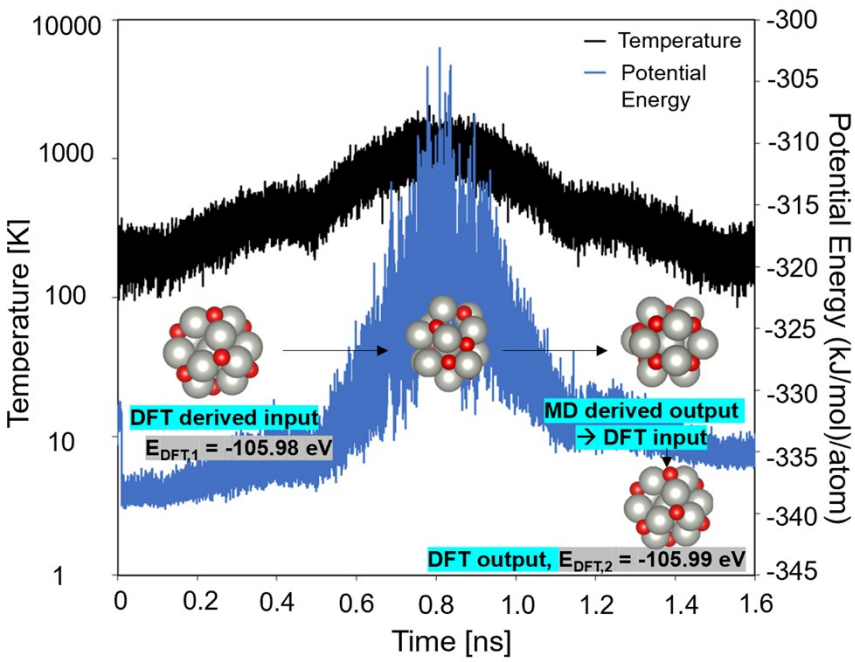

Figure S7. An example of a DFT/MD/DFT run with ReaxFF annealing calculation for $Pd_{13}O_8$, where temperature is the black curve and potential energy is the blue curve. This demonstrates method 1 for PdO cluster construction, as described in Fig. S1.

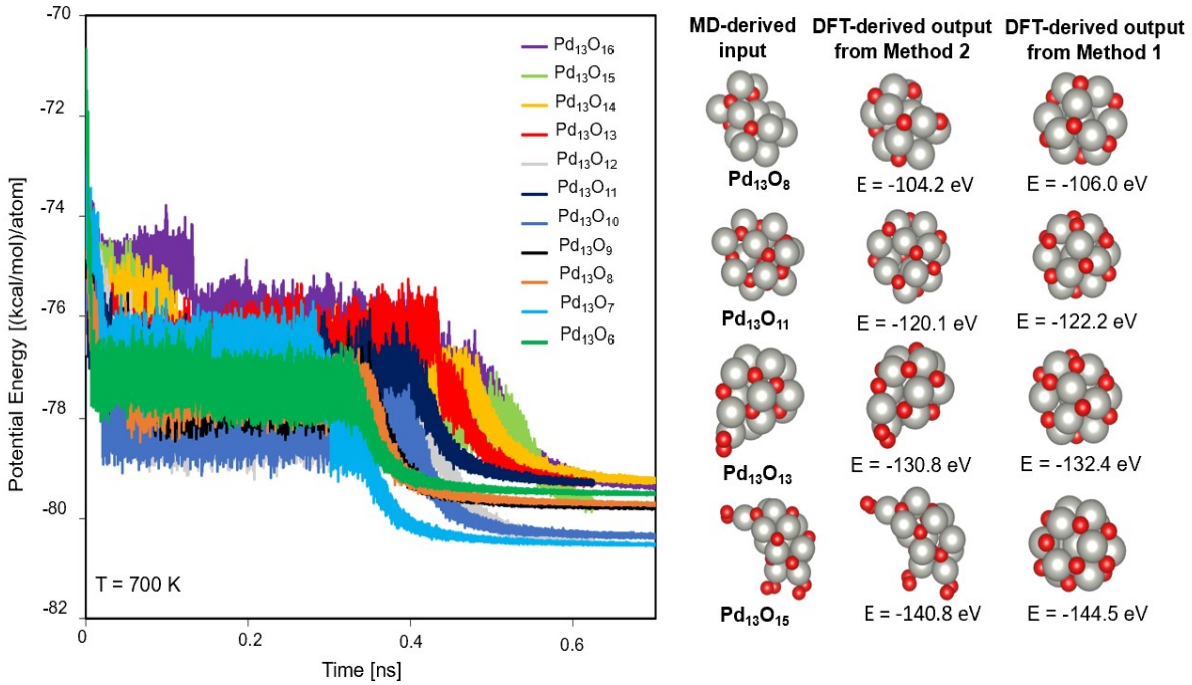

Figure S8. Potential energy curves for $Pd_{13}O_y$ clusters constructed using constant temperature ReaxFF simulations (method 2, Fig. S1). These clusters were compared with those found using method 1 and the lower energy cluster was used for further DFT calculations.

S2. Ab-initio thermodynamic calculations

(a) Other contributions to the Helmholtz free energy

Within the grand canonical ensemble, the number of particles fluctuates to minimize the grand potential (Φ) at a given set of reaction conditions (oxygen and Pd chemical potentials) as shown below.

$$\Phi_{N_{Pd}N_O}(T,\mu_{Pd*},\mu_{O*}) = F_{N_{Pd}N_O}(T) - N_{Pd}\mu_{Pd*} - N_O\mu_{O*} \qquad (S1)$$

Here, $\Phi_{N_{Pd}N_O}$ is the grand potential of the system with N_i numbers of Pd and O atoms and μ_{i*} is the chemical potential of bound species i. $F_{N_{Pd}N_O}$ represents the Helmholtz free energy, which includes the internal energy of the Pd, PdO/Pd, and PdO structures (approximated as its electronic energy derived from DFT methods, $E^{DFT}_{N_{Pd}N_O}$), the vibrational contributions to the Helmholtz free energy ($F^{vib}_{N_{Pd}N_O}(T)$), and the configurational entropic contribution to the Helmholtz free energy (S^{conf}) at a given temperature T:

$$F_{N_{Pd}N_O}(T) = E^{DFT}_{N_{Pd}N_O} + F^{vib}_{N_{Pd}N_O}(T) - TS^{conf} \qquad (S2)$$

The effect of vibrational contributions to the Helmholtz free energy ($F^{vib}_{N_{Pd}N_O}(T)$) was estimated based on the method proposed by Reuter et al.[5–7] To avoid using computationally intensive phonon density of states (DOS) calculations, the Einstein model was employed. This model considers one characteristic frequency, w, for each atom type (i.e. chemisorbed atom, gas phase atoms, and atoms in the bulk). Thus,

$$F^{vib}_{N_{Pd}N_O}(T) = \frac{hw}{2} + kTln\left(1 - e^{\frac{-hw}{kT}}\right) \qquad (S3)$$

where h is Planck's constant, k is the Boltzmann constant, and T is the temperature. Since we are only considering the relative grand potential between the clean and oxidized surface, allowing this frequency to change significantly for surface O* atoms compared to those in the solid bulk or in the gas phase provides an order of magnitude estimate of the vibrational contribution. Thus, the relative vibrational frequency between chemisorbed oxygen on the surface and gas phase oxygen can be calculated as:

$$\Delta F^{vib}_{N_{Pd}N_O} = -\frac{1}{A}\left(F^{vib}(T,w) - \frac{1}{2}F^{vib}(<w>)\right) \qquad (S4)$$

Here, w is the characteristic frequency of the vertical stretch of the O/Pd bond (80 meV) and $<w>$ is the characteristic frequency of oxygen in the gas phase (196 meV). Considering the potential errors accumulated in calculating the characteristic surface frequency, this frequency was also varied +/- 50% of the original value. As seen in Fig. S9a, even for extensive variations of the characteristic vibrational modes

(shown as dashed lines), the resulting vibrational contribution stays within +/- 10 meV/ Å^2 for the temperature range considered.

Configurational entropic effects were calculated based on the method proposed by Reuter et al. If a system with N number of surface sites has a small number of n defects or adsorbate sites (n << N), the configurational entropy is given by

$$S^{conf} = kln\frac{(N+n)!}{N!n!} \qquad (S5)$$

If A_{site} is the surface area per site, the configurational entropy per surface area is

$$\frac{TS^{conf}}{NA_{site}} = \frac{kT}{NA_{site}}ln\frac{(N+n)!}{N!n!} \qquad (S6)$$

Then, if N and n are much greater than 1, then the Stirling formula can be applied:

$$\frac{TS^{conf}}{NA_{site}} = \frac{kT}{A_{site}}\left[\ln\left(1+\frac{n}{N}\right)+\left(\frac{n}{N}\right)\ln\left(1+\frac{n}{N}\right)\right] \qquad (S7)$$

The expression in the brackets varies between 0 for n/N = 0 and 0.34 for n/N = 0.1 (10 %). Therefore, the configurational entropy can be approximated as

$$\frac{TS^{conf}}{NA_{site}} = 0.34\frac{kT}{A_{site}} \qquad (S8)$$

Assuming a typical area per surface site of 10 Å^2 for transition metal surfaces, the configurational entropic contribution was found to be less than 3 meV/Å^2 for a temperature range of 100 to 1000 K (Fig. S9b).

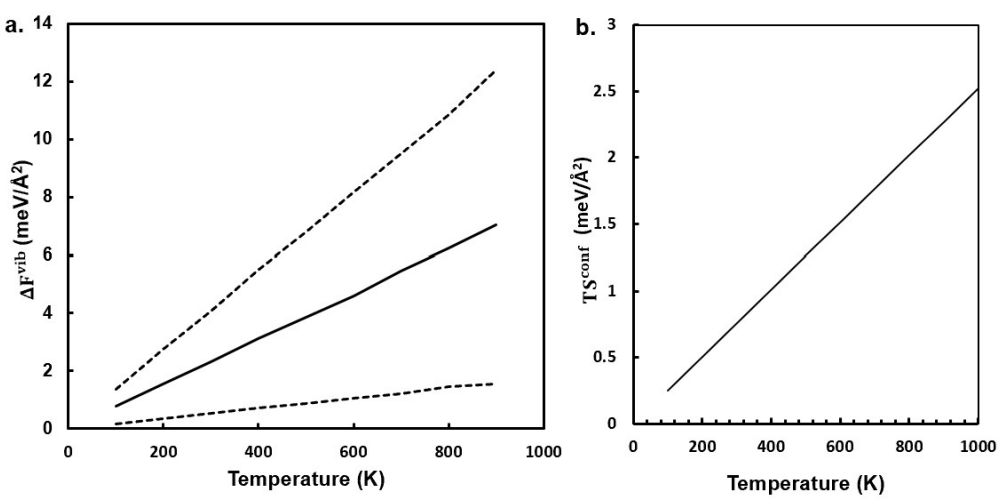

Figure S9: The contributions of (a) vibrational free energies, where the characteristic vibrational mode was varied +/- 50% of the original value (shown as dashed lines), and (b) configurational free energies to the total free energy at a temperature range of 100-1000 K.

Table S1: Reference chemical potential for gas phase species (1/2 O_2, H_2O, H_2O_2, and H_2), calculated using JANAF thermochemical tables.

P_0 = 100000 Pa	$1/2O_2$	H_2O	H_2O_2	H_2
T [K]	μ_i^o[eV]	μ_i^o [eV]	μ_i^o [eV]	μ_i^o [eV]
100	-0.075	-0.124	-0.159	-0.036
200	-0.170	-0.295	-0.362	-0.094
300	-0.274	-0.485	-0.612	-0.159
400	-0.383	-0.686	-0.861	-0.229
500	-0.495	-0.896	-1.12	-0.303
600	-0.611	-1.11	-1.39	-0.380
700	-0.730	-1.34	-1.68	-0.460
800	-0.851	-1.57	-1.97	-0.541
900	-0.974	-1.8	-2.27	-0.625
1000	-1.10	-2.04	-2.57	-0.710

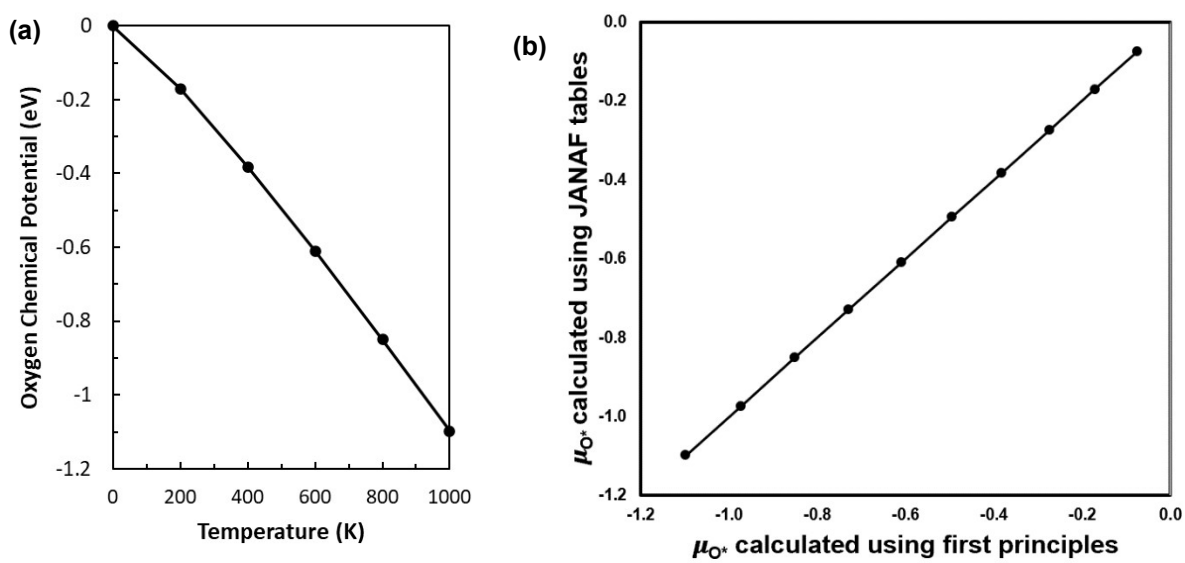

Figure S10. (a) Temperature dependence of the oxygen chemical potential ($\mu_{O^*}^o$) at p=1 bar calculated using first principles. (b) Comparison between $\mu_{O^*}^o$ calculated using either JANAF thermochemical tables or first principles.[8]

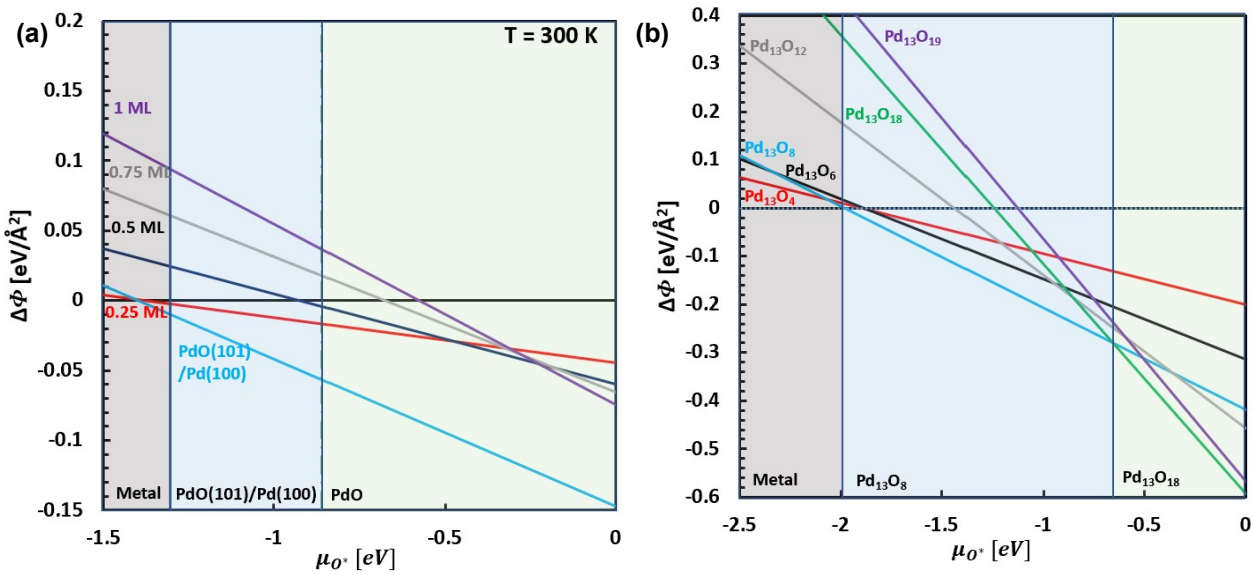

Figure S11. Surface phase diagrams of (a) Pd(100) and (b) Pd_{13} as a function of the chemical potential of O* (μ_{O*}^{o}) at T = 300 K. The stable phases are represented by blocks of color, where the stable phase occurs at the intersection of each line at which the relative grand potential becomes more negative.

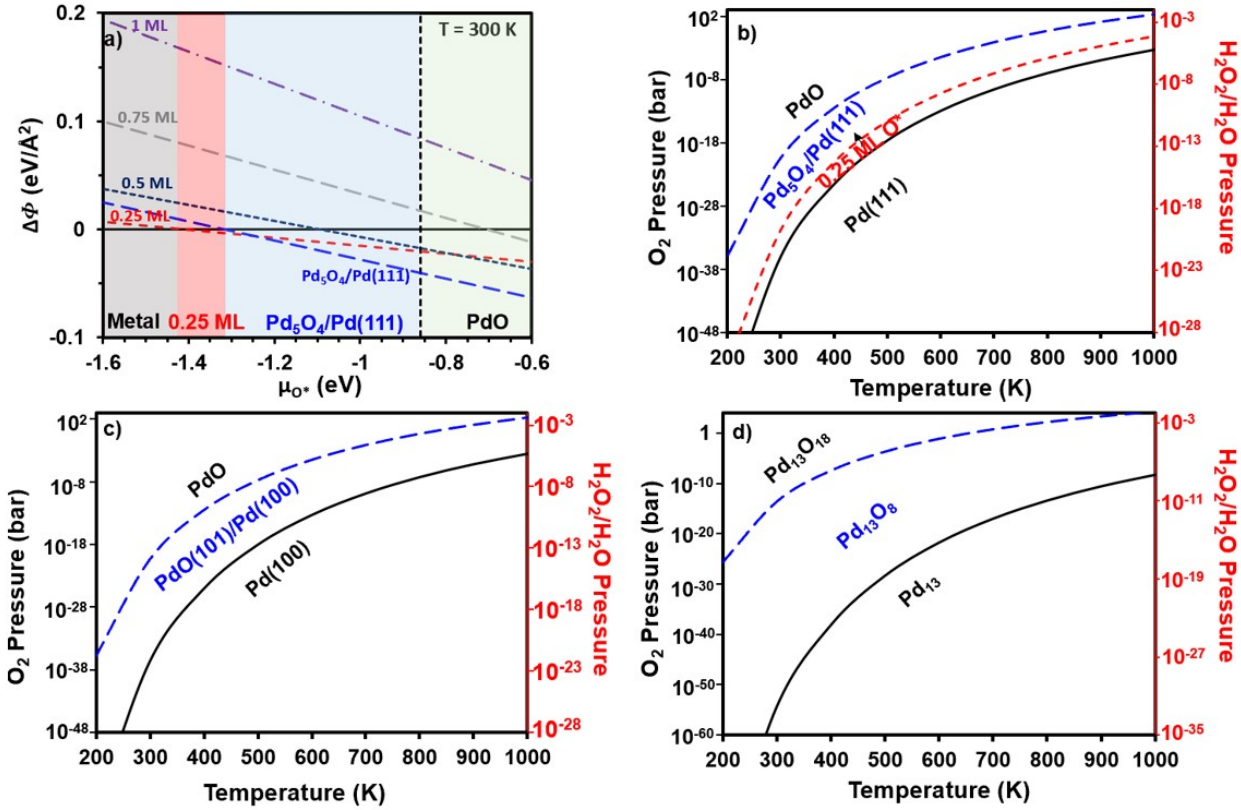

Figure S12. a) Surface phase diagram of Pd(111) in terms of the chemical potential of O* (μ_{O*}^{o}) at T = 300 K. The corresponding T, p diagrams denoting the stable regions of each structure over a range of temperatures (200-1000K) and H_2O_2/H_2O and O_2 pressures (bar) for b) Pd(111), c) Pd(100), and d) Pd_{13}.

(b) Phase diagrams in O_2/H_2 environments

The surface phase diagram for Pd(111) in O_2/H_2 environments is derived based on ab initio thermodynamics. The grand potential (Φ) within the grand canonical ensemble depends on the chemical potentials of Pd*, O*, and H* species:

$$\Phi_{N_{Pd}N_O N_H}(T,\mu_{Pd*},\mu_{O*},\mu_{H*}) = F_{N_{Pd}N_O N_H}(T) - N_{Pd}\mu_{Pd*} - N_O\mu_{O*} - N_O\mu_{H*} \qquad (S9)$$

In thermodynamic equilibrium, the chemical potentials of O* and H* in the solid are set by the chemical potentials of gas phase O_2 and H_2:

$$\mu_{O*} = \frac{1}{2}\mu_{O_2} \qquad (S10)$$

$$\mu_{H*} = \frac{1}{2}\mu_{H_2} \qquad (S11)$$

The chemical potential of a gas-phase species *i*, μ_i, can be calculated as:

$$\mu_i = \mu_i^o + k_B T ln\left(\frac{p_i}{p^0}\right) \qquad (S12)$$

where p_i is the partial pressure and μ_i^o is reference chemical potential (calculated with the standard enthalpy and entropy values listed in the JANAF thermochemical tables; Table S1).

The lower limit of μ_{O*} is set under oxidant-poor conditions at which the bulk oxide decomposes into gas-phase oxidant and metallic Pd:

$$\mu_{PdO}^{bulk} < \mu_{Pd}^{bulk} + \frac{1}{2}\mu_{O_2} \qquad (S13)$$

At T = 0 K, the Gibbs free energy of formation for PdO ($\Delta G_{f,PdO}$) is given by $\mu_{PdO}^{bulk} - \mu_{Pd}^{bulk} - \frac{1}{2}\mu_{O_2}$, which can be approximated with DFT-derived electronic energies.

$$\Delta G_{f,PdO} = E_{PdO}^{DFT} - E_{Pd}^{DFT} - \frac{1}{2}(E_{O_2}^{DFT} + E_{O_2}^{ZPVE}) = -0.87\ eV \qquad (S14)$$

DFT-derived value of $\Delta G_{f,PdO}$ (-0.87 eV) agrees relatively well with the experimental value for $\Delta G_{f,PdO}$ of -0.97 eV and thus has been used as the boundary conditions. Within O_2 and H_2 mixtures, PdO is reduced into Pd and H_2O at higher H_2/O_2 ratios, which gives a second boundary condition:

$$\mu_{Pd}^{bulk} + \mu_{H_2O} < \mu_{PdO}^{bulk} + \mu_{H_2} \qquad (S14)$$

The stability criterion for PdO in O_2/H_2 environments is then given by combining Equations S12, S13 and S14:

$$\Delta\mu_{H_2} - \frac{1}{2}\mu_{O_2} < -2\,\Delta G_{f,\,PdO} + \Delta G_{f,H_2O} \quad , \qquad (S14)$$

where $\Delta G_{f,H_2O}$, the Gibbs free energy of formation for H_2O from H_2 and O_2, was calculated to be -2.55 eV from DFT-derived electronic energies. The surface phase diagrams for Pd(111) in O_2/H_2 environments (shown in Figure S13) are derived by calculating the change in the grand potential ($\Delta\Phi$) over a range of $\mu_{O_2}$and $\mu_{H_2}$for different Pd-O systems relative to clean models and identifying the configurations that minimize $\Delta\Phi$ using Eq. S9. The pressure bars are set by holding temperature constant and using Eq. S12 to calculate the pressure at specific O_2 and H_2 chemical potentials.

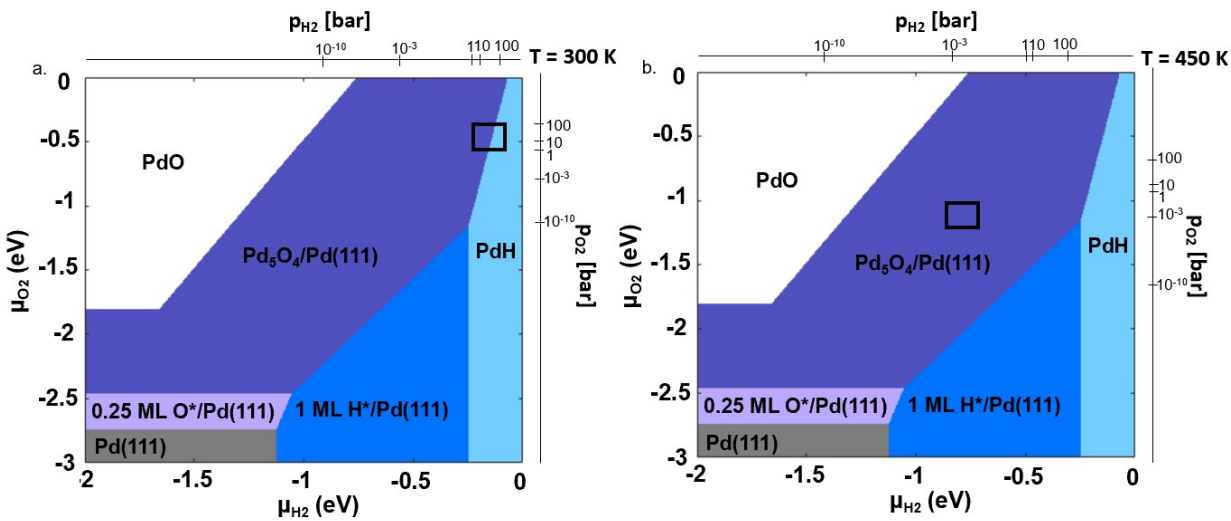

Figure S13. Surface phase diagram of Pd(111) as a function of chemical potentials of H_2(g) and O_2(g) at (a) 300 K and (b) 450 K. The black boxes represent typical operating conditions during (a) H_2O_2 synthesis (P_{H_2}, P_{O_2} = 5-100 bar, T = 275-315 K)[9] and (b) C_3H_8 oxidation reaction with H_2 and O_2 co-feed (P_{H_2}, P_{O_2} = 10^{-3}-1 bar, T = 450 K)[10]

S3. DFT assessments of adsorbate binding on all surfaces and clusters

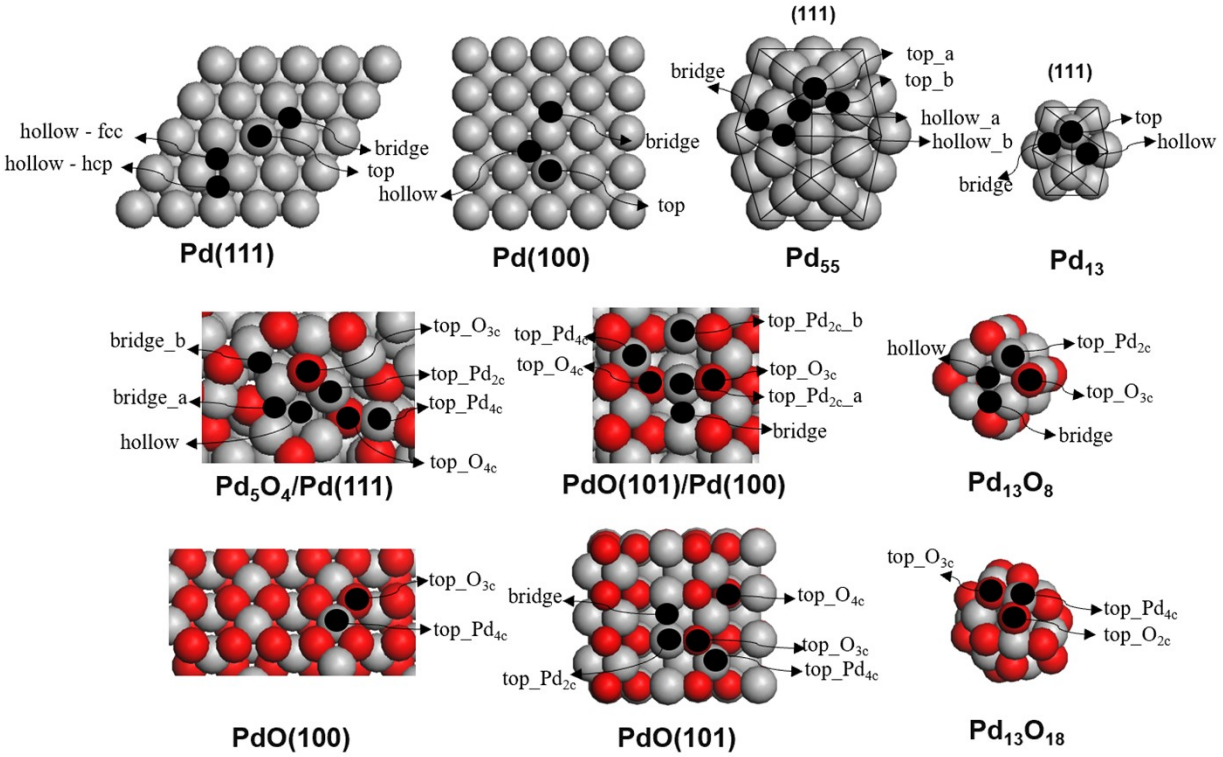

Figure S14. Possible binding sites in Pd(111), Pd(100), Pd_{55}, Pd_{13}, Pd_5O_4/Pd(111), PdO(100), PdO(101), $Pd_{13}O_8$, and $Pd_{13}O_{18}$ models and their nomenclatures.

Table S2. DFT-derived adsorption energies (kJ mol^{-1}) of adsorbed species on the Pd(100) surface. Adsorption energies calculated from this work (PBE-D2) were compared to those in the literature (PW91).

	Pd(100)	PBE-D2	PW91 [ref[11]]
Species	Binding Site	(kJ/mol)	(kJ/mol)
O*	Hollow	-466	-376
O*	Bridge	-430	
H*	Hollow	-370	-264
H*	Bridge	-367	
OH*	Bridge-tilted	-294	-210
OH*	Hollow	-280	
OOH*	Bent-bridge	-186	-123
H_2O_2*	Top	-79	-35
H_2O*	Top	-61	-29
O_2*	Hollow	-172	-123

*all adsorption energies are electronic energies without any corrections and referenced to the corresponding molecules in the gas-phase (e.g., O(g), H(g), OH(g), OOH(g), H_2O(g), H_2O_2(g)). Relevant adsorption configurations are shown in Figure S15.

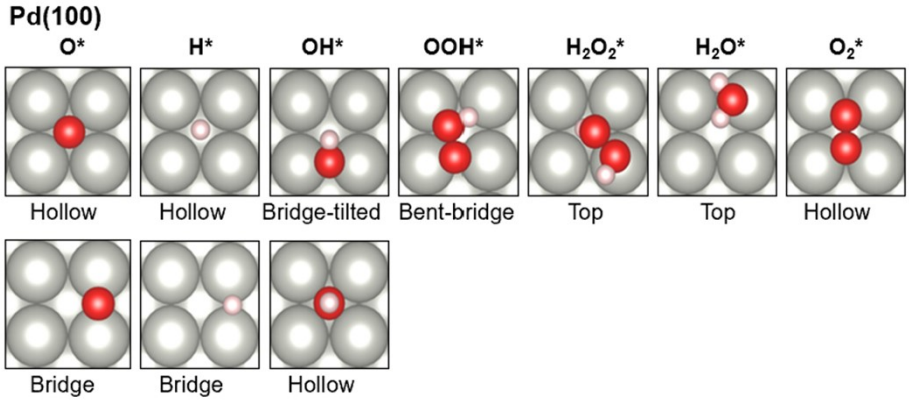

Figure S15. DFT-derived adsorption configurations of adsorbed species on the Pd(100) surface.

Table S3. DFT-derived adsorption energies (kJ mol^{-1}) of adsorbed species on the Pd(111) surface. Adsorption energies calculated from this work (PBE-D2) were compared to those in the literature (PW91).

	Pd(111)	PBE-D2	PW91[ref [11]]
Species	Binding Site	(kJ/mol)	(kJ/mol)
O*	Hollow - fcc	-464	-351
O*	Hollow - hcp	-430	
O*	Top	-317	
H*	Hollow - fcc	-381	
H*	Hollow - hcp	-361	-260
H*	Bridge	-367	
H*	Top	-330	
OH*	Bridge-tilted	-260	-196
OH*	Hollow - fcc	-253	
OH*	Hollow - hcp	-238	
OOH*	Bent-top	-126	-91
H_2O_2*	Top	-67	-31
H_2O*	Top	-51	-21
O_2*	Top-bridge	-99	-48

*all adsorption energies are electronic energies without any corrections and referenced to the corresponding molecule in the gas-phase (e.g., O(g), H(g), OH(g), OOH(g), H_2O(g), H_2O_2(g)) Relevant adsorption configurations are shown in Figure S16.

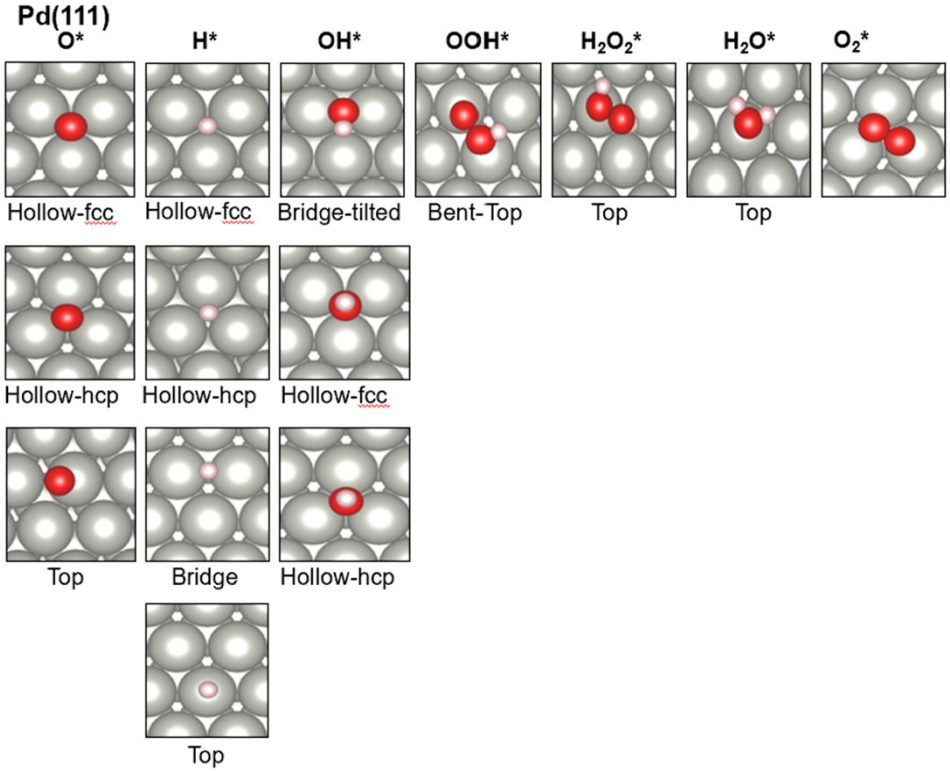

Figure S16. DFT-derived adsorption configurations of adsorbed species on Pd(111).

Table S4. DFT-derived adsorption energies (kJ mol^{-1}) of adsorbed species on the Pd_{13} cluster.

	Pd_{13}	
Species	Binding Site	(kJ/mol)
O*	Hollow	-469
O*	Bridge	-448
O*	Top	-370
H*	Hollow	-419
H*	Bridge	-413
OH*	Bridge-tilted	-326
OH*	Hollow	-314
OH*	Top-tilted	-299
OOH*	Bent-top	-212
H_2O_2*	Top	-99
H_2O*	Top	-86
O_2*	Top-bridge	-190

*all adsorption energies are electronic energies without any corrections and referenced to the corresponding molecule in the gas-phase (e.g., O(g), H(g), OH(g), OOH(g), H_2O(g), H_2O_2(g)) Relevant adsorption configurations are shown in Figure S17.

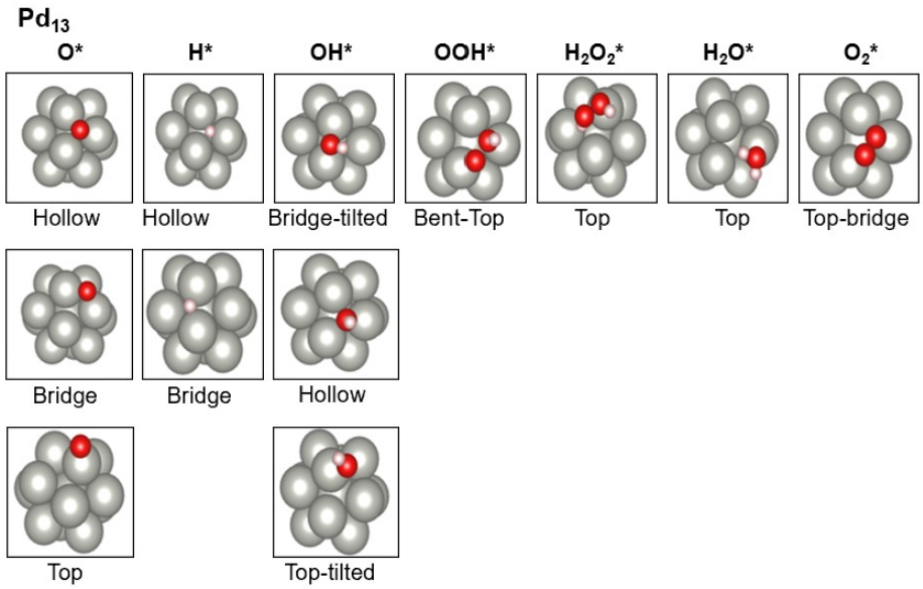

Figure S17. DFT-derived adsorption configurations of adsorbed species on the Pd_{13} cluster.

Table S5. DFT-derived adsorption energies (kJ mol^{-1}) of adsorbed species on the on the Pd_{55} cluster.

	Pd_{55}	
Species	Binding Site	(kJ/mol)
O*	Hollow_a	-493
O*	Hollow_b	-483
O*	Top	-384
H*	Hollow_b	-388
H*	Hollow_a	-386
H*	Bridge	-378
H*	Top	-324
H*	Top_1	-337
OH*	Bridge_1	-294
OH*	Bridge_2	-276
OH*	Hollow_b	-285
OH*	Hollow_a	-289
OOH*	Top	-192
H_2O_2*	Top_1	-71
H_2O_2*	Top_2	-69
H_2O*	Top_1	-59
H_2O*	Top_2	-55
O_2*	Top	-156

*all adsorption energies are electronic energies without any corrections and referenced to the corresponding molecule in the gas-phase (e.g., O(g), H(g), OH(g), OOH(g), H_2O(g), H_2O_2(g)) Relevant adsorption configurations are shown in Figure S18.

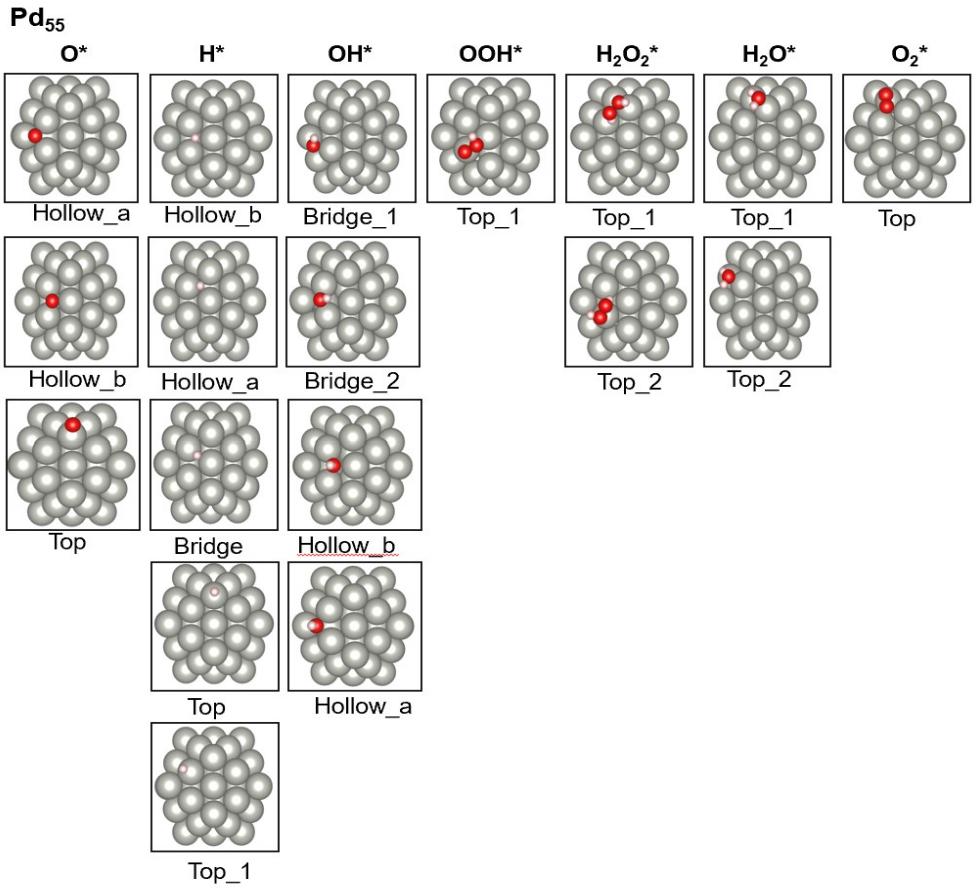

Figure S18. DFT-derived adsorption configurations of adsorbed species on the Pd_{55} cluster.

Table S6. DFT-derived adsorption energies (kJ mol^{-1}) of adsorbed species on the on Pd_5O_4/Pd(111).

	Pd_5O_4/Pd(111)	
Species	Binding Site	(kJ/mol)
O*	Bridge_a	-314
O*	Bridge_b	-295
O*	Hollow	-312
H*	Top – O_{3c}	-364
OH*	Bridge_a	-223
OH*	Bridge_b	-213
OH*	Bridge_b_1	-209
OOH*	Bidentate	-124
OOH*	Bidentate_1	-110
OOH*	Bridge_a	-132
OOH*	Top	-104
OOH*	Bidentate_2	-123
OOH*	Bridge_b	-118
OOH*	Bridge_a_2	-122
H_2O_2*	Top_1	-68
H_2O_2*	Top_2	-48
H_2O*	Top_1	-38
H_2O*	Top_2	-39
O_2*	Bridge_a	-60
O_2*	Bidentate	-52
O_2*	Bidentate_1	-30
O_2*	Top	-25
O_2*	Hollow	-43

*all adsorption energies are electronic energies without any corrections and referenced to the corresponding molecule in the gas-phase (e.g., O(g), H(g), OH(g), OOH(g), H_2O(g), H_2O_2(g)) Relevant adsorption configurations are shown in Figure S19.

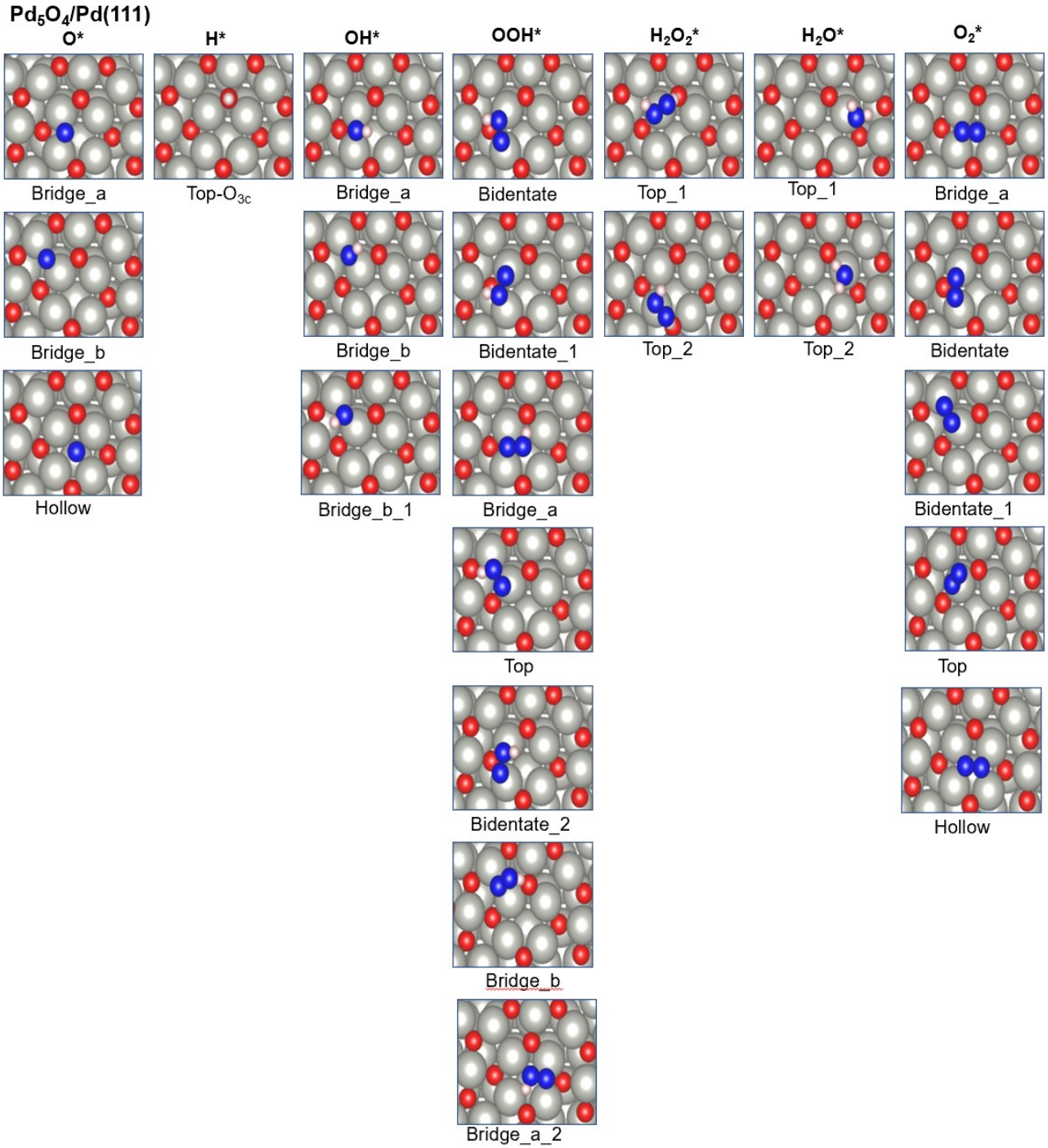

Figure S19: DFT-derived binding configurations of adsorbed species on Pd_5O_4/Pd(111).

Table S7. DFT-derived adsorption energies (kJ mol^{-1}) of adsorbed species on the on PdO(101)/Pd(100).

	PdO(101)-Pd(100)	
Species	Binding Site	(kJ/mol)
O*	Bridge_a	-339
O*	Bridge_b	-334
O*	Top	-239
H*	Top_O_{3c}_1	-383
H*	Top_O_{3c}_2	-376
H*	Top_O_{4c}	-307
OH*	Bridge_b	-255
OH*	Bridge_a	-256
OOH*	Bidentate_1	-100
OOH*	Bidentate_2	-108
OOH*	Bidentate_3	-124
OOH*	Bidentate_4	-126
OOH*	Top	-124
OOH*	Bridge	-155
H_2O_2*	Top_1	-67
H_2O_2*	Top_2	-62
H_2O*	Top_1	-42
H_2O*	Top_2	-35
H_2O*	Top_3	-33
H_2O*	Top_4	-36
O_2*	Top_1	-25
O_2*	Top_2	-27
O_2*	Bidentate_1	-42
O_2*	Bidentate_2	-39
O_2*	Bridge	-25

*all adsorption energies are electronic energies without any corrections and referenced to the corresponding molecule in the gas-phase (e.g., O(g), H(g), OH(g), OOH(g), H_2O(g), H_2O_2(g)) Relevant adsorption configurations are shown in Figure S20.

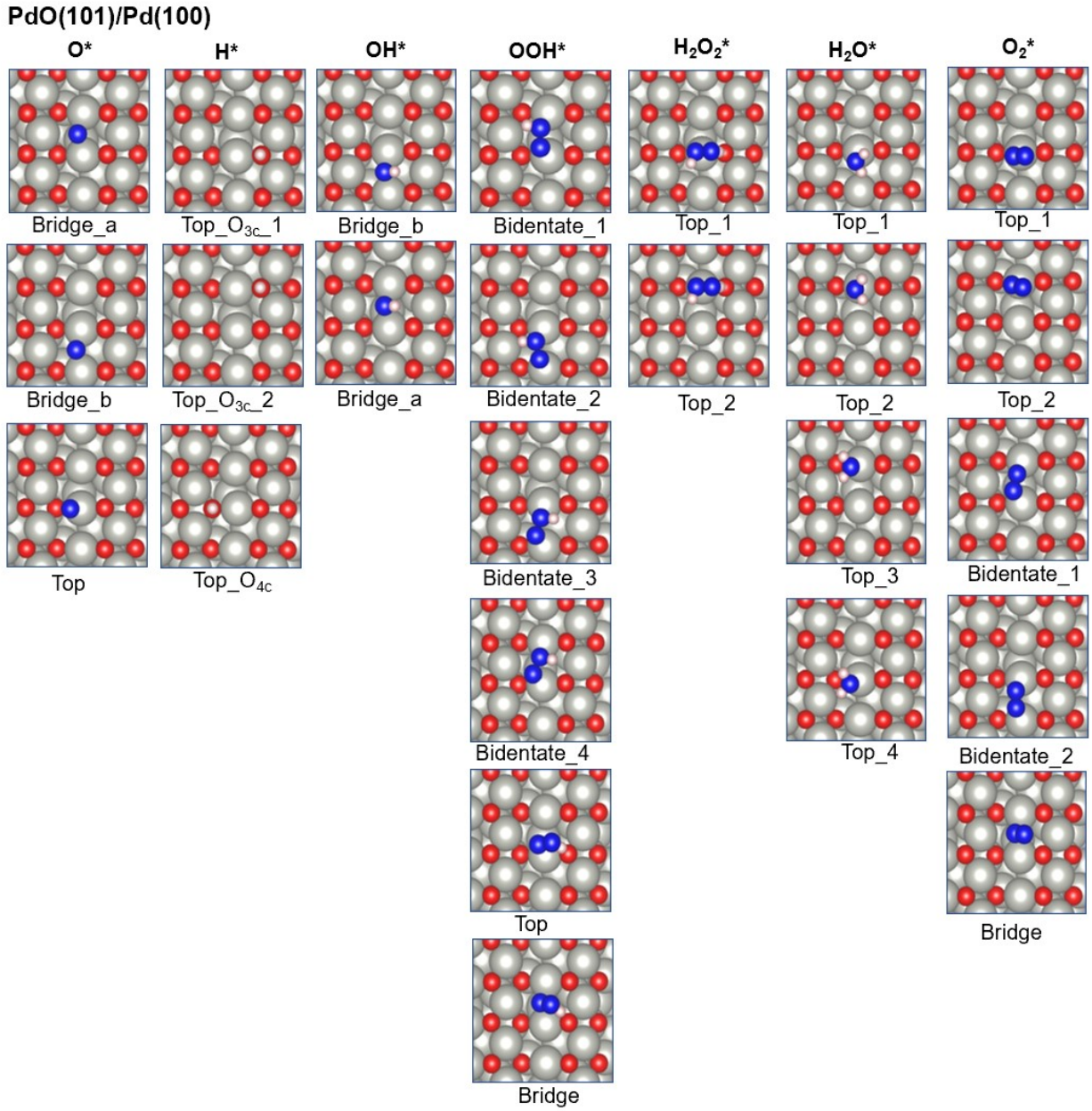

Figure S20. DFT-derived binding configurations of adsorbed species on PdO(101)/Pd(100).

Table S8. DFT-derived adsorption energies (kJ mol^{-1}) of adsorbed species on the $Pd_{13}O_8$ cluster.

	$Pd_{13}O_8$	
Species	Binding Site	(kJ/mol)
O*	Bridge	-285
O*	Top	-251
O*	4-fold hollow	-286
H*	Top - O	-405
H*	Top – Pd	-304
H*	Hollow	-343
OH*	Top - tilted	-196
OH*	Bridge - tilted	-205
OH*	Hollow	-169
OOH*	Top -bridge	-103
OOH*	Top	-110
OOH*	Top	-113
OOH*	Bridge	-102
H_2O_2*	Top_1	-68
H_2O_2*	Top_2	-49
H_2O*	Top	-34
H_2O*	Top	-39
O_2*	Hollow	-32
O_2*	Bridge	-54

*all adsorption energies are electronic energies without any corrections and referenced to the corresponding molecule in the gas-phase (e.g., O(g), H(g), OH(g), OOH(g), H_2O(g), H_2O_2(g)) Relevant adsorption configurations are shown in Figure S21.

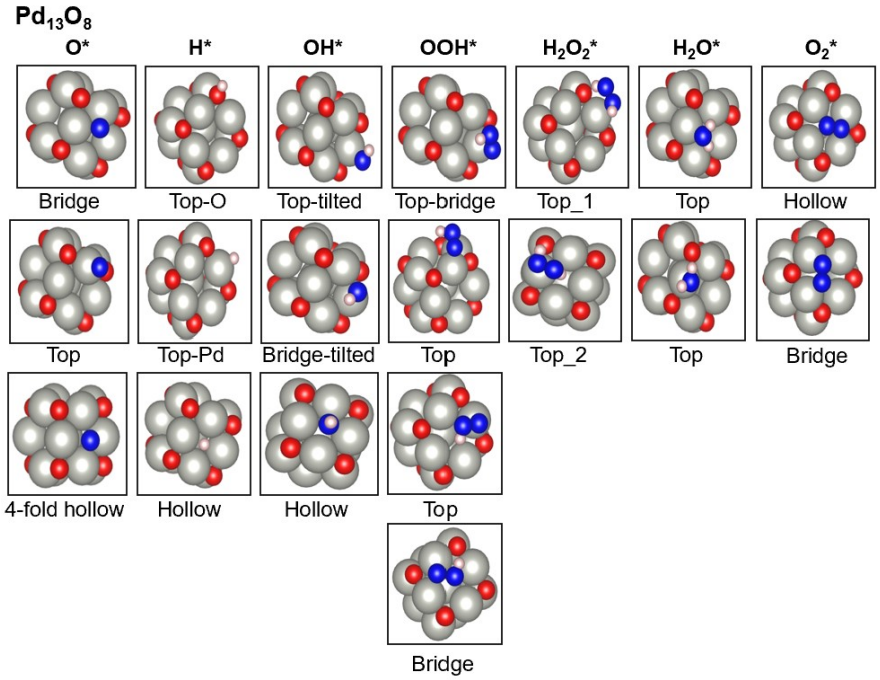

Figure S21. DFT-derived configurations of adsorbed species on the $Pd_{13}O_8$ cluster.

Table S9. DFT-derived adsorption energies (kJ mol^{-1}) of adsorbed species on the on the PdO(101) surface.

	PdO(101)	
Species	Binding Site	(kJ/mol)
O*	Top	-328
O*	Bridge	-375
H*	Top - O	-395
H*	Top - Pd	-27
OH*	Top - tilted	-284
OH*	Top - tilted	-272
OH*	Bridge	-304
OOH*	Bridge - tilted	-239
OOH*	Top	-194
OOH*	Bidentate	-219
H_2O_2*	Top	-118
H_2O*	Top	-94
O_2*	Bidentate	-142
O_2*	Bridge	-64
O_2*	Top	-85

*all adsorption energies are electronic energies without any corrections and referenced to the corresponding molecule in the gas-phase (e.g., O(g), H(g), OH(g), OOH(g), H_2O(g), H_2O_2(g)) Relevant adsorption configurations are shown in Figure S22.

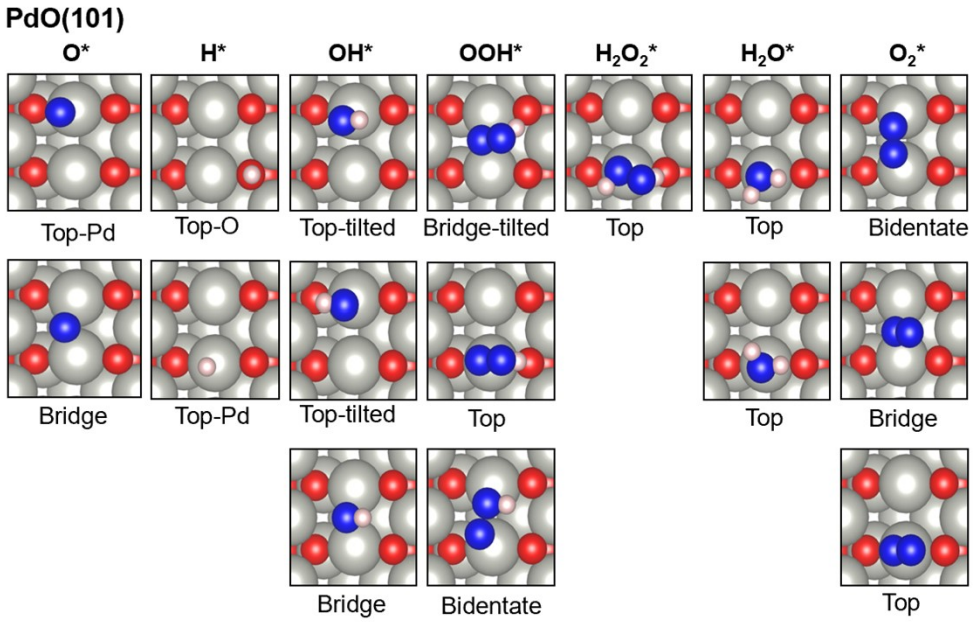

Figure S22. DFT-derived binding configurations of adsorbed species on the PdO(101) surface.

Table S10. DFT-derived adsorption energies (kJ mol^{-1}) of adsorbed species on the PdO(100) surface.

	PdO(100)	
Species	Binding Site	(kJ/mol)
O*	Top	-170
H*	Top - O	-448
H*	Top - Pd	26
OH*	Top - tilted	-154
OOH*	Top	-101
OOH*	Top_1	-92
H_2O_2*	Top_1	-64
H_2O_2*	Top_2	-70
H_2O*	Top	-33
O_2*	Top_1	-24
O_2*	Top_2	-20

*all adsorption energies are electronic energies without any corrections and referenced to the corresponding molecule in the gas-phase (e.g., O(g), H(g), OH(g), OOH(g), H_2O(g), H_2O_2(g)) Relevant adsorption configurations are shown in Figure S23.

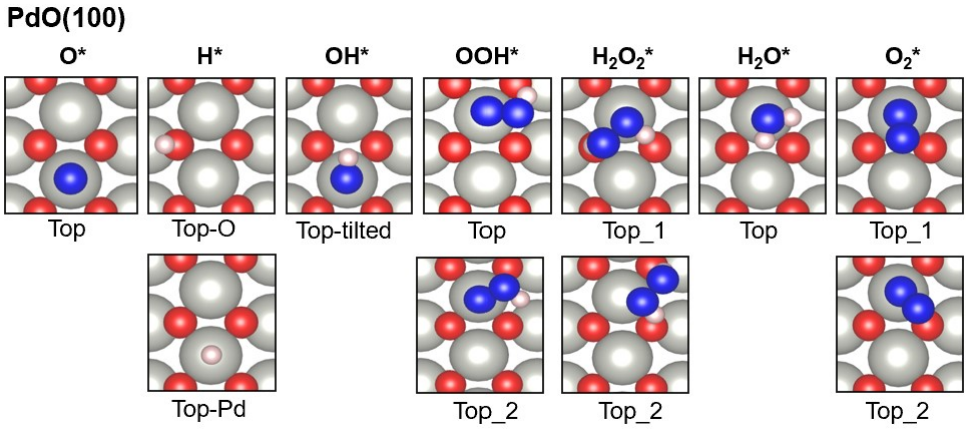

Figure S23. DFT-derived binding configurations of adsorbed species on the PdO(100) surface.

Table S11. DFT-derived adsorption energies (kJ mol^{-1}) of adsorbed species on the $Pd_{13}O_{18,}$ cluster.

	$Pd_{13}O_{18}$	PBE-D2
Species	Binding Site	BE (kJ/mol)
O*	Top	-207
H*	Top – O_{2c}	-503
H*	Top – O_{3c}	-466
OH*	Top - tilted	-160
OH*	Top – tilted_1	-167
OOH*	Top	-89
H_2O_2*	Top_1	-65
H_2O_2*	Top_2	-56
H_2O_2*	Top_3	-57
H_2O_2*	Top_4	-54
H_2O*	Top	-38
O_2*	Top_1	-20
O_2*	Top_2	-22
O_2*	Top_3	-23

*all adsorption energies are electronic energies without any corrections and referenced to the corresponding molecule in the gas-phase (e.g., O(g), H(g), OH(g), OOH(g), H_2O(g), H_2O_2(g)) Relevant adsorption configurations are shown in Figure S24.

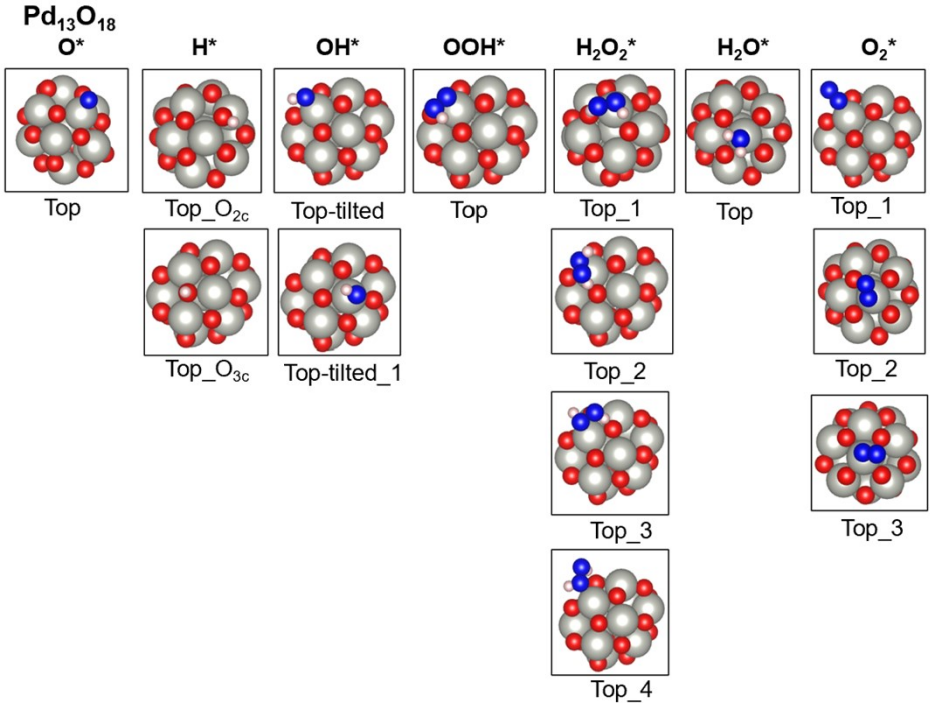

Figure S24. DFT-derived binding configurations of adsorbed species on the $Pd_{13}O_{18}$ cluster.

S4. H_2O_2 Synthesis and Decomposition Reaction Energy Pathways for Pd and PdO/Pd and PdO surfaces

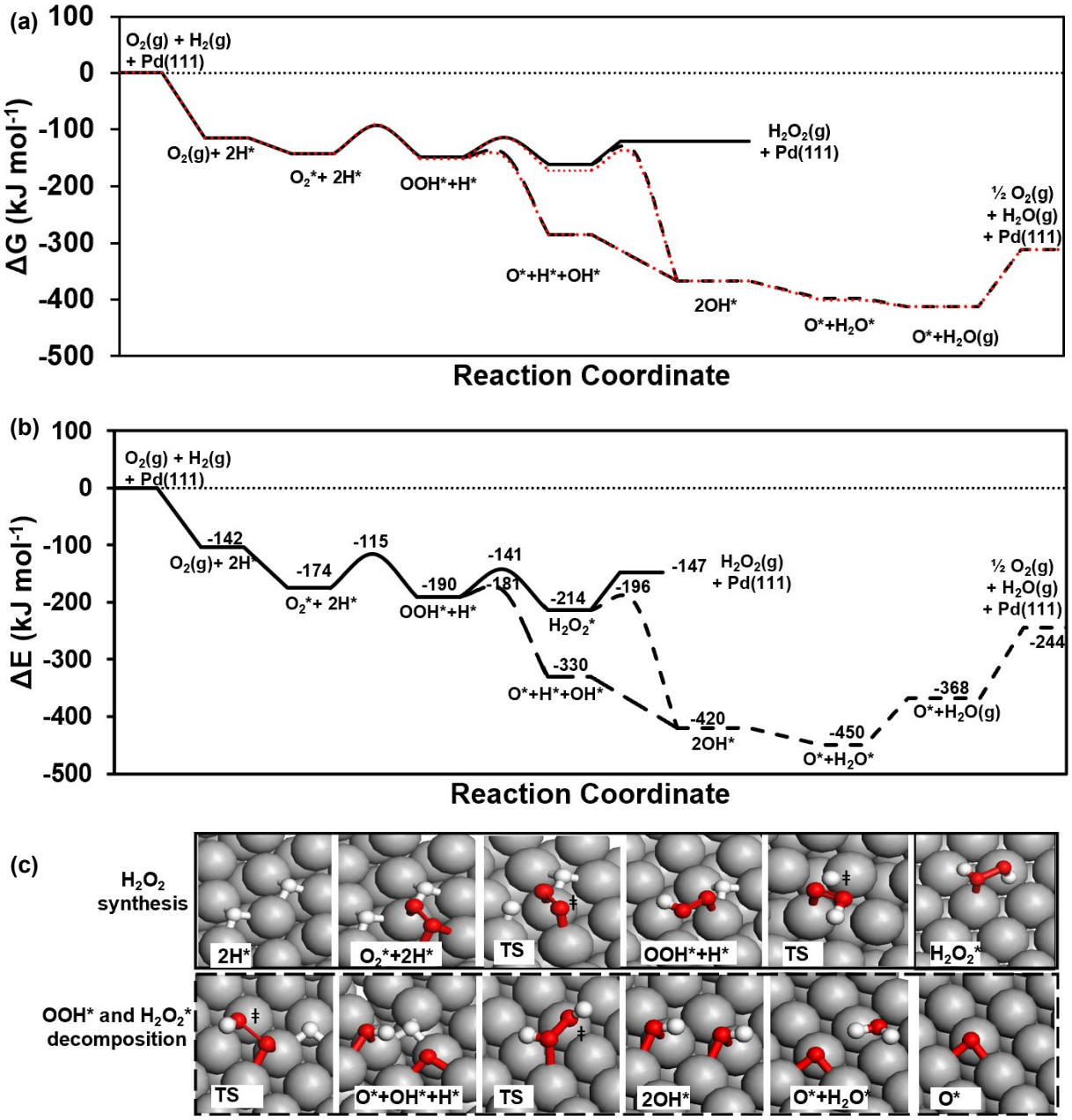

Figure S25. DFT-derived (a) Gibbs free energies, (b) electronic energies, (c) structures of intermediates and TS structures involved in the possible H_2O_2 synthesis pathways on Pd(111) (in Scheme 1). All energies are reference to the energies of O_2(g) and H_2(g) and clean Pd(111) surface. Low vibrational modes (< 100 cm^{-1}) are either replaced by a 70% contribution of the average of translational and rotational entropy of the molecule in the gas phase (red dashed lines in Panel (a)) or deleted in (black lines in Panel (a)) in calculating entropies of weakly bound intermediates and TS.

.

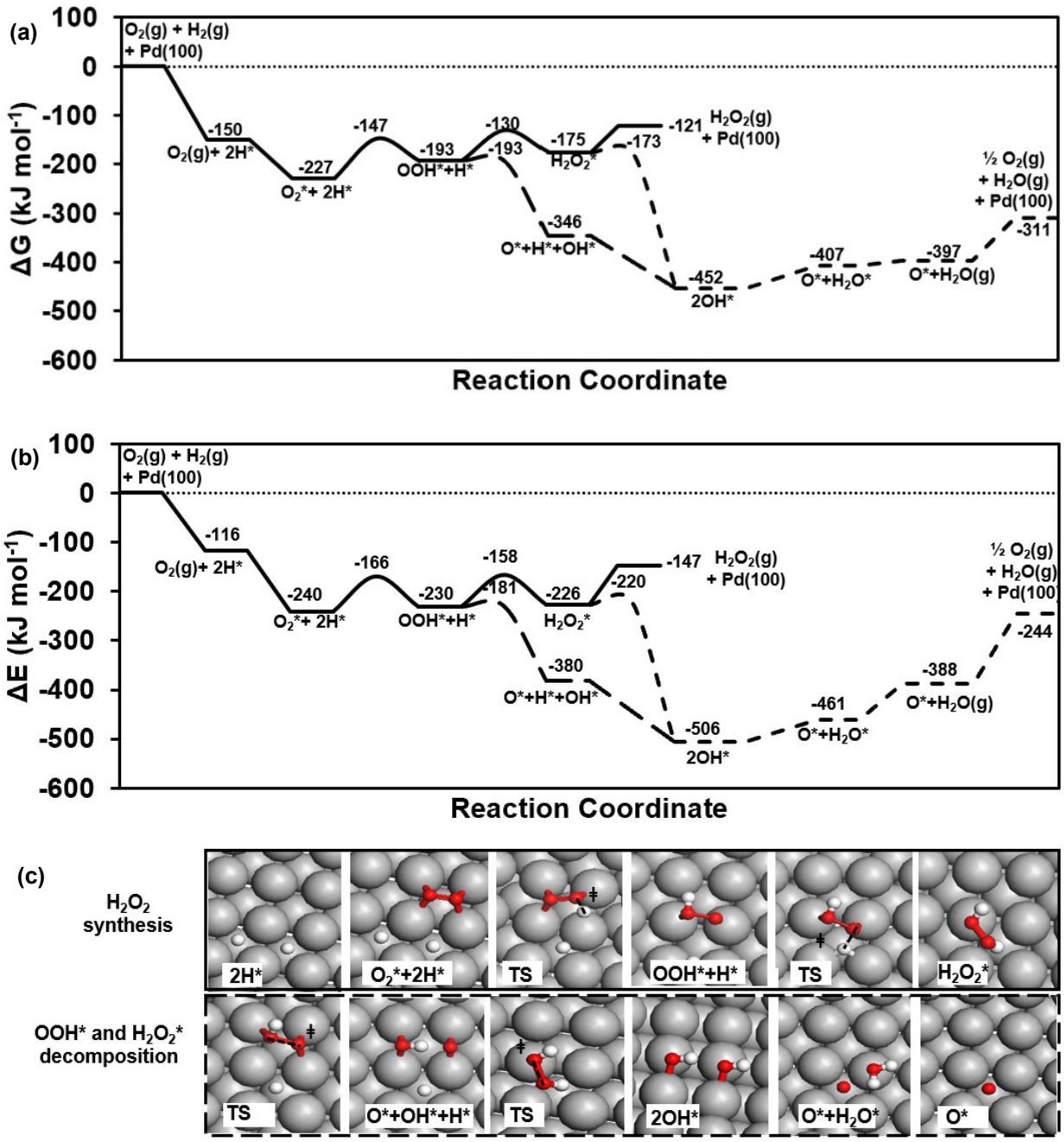

Figure S26. DFT-derived (a) Gibbs free energies, (b) electronic energies, (c) structures of intermediates and TS structures involved in the possible H_2O_2 synthesis pathways on Pd(100) (in Scheme 1). All energies are reference to the energies of O_2(g) and H_2(g) and clean Pd(100) surface.

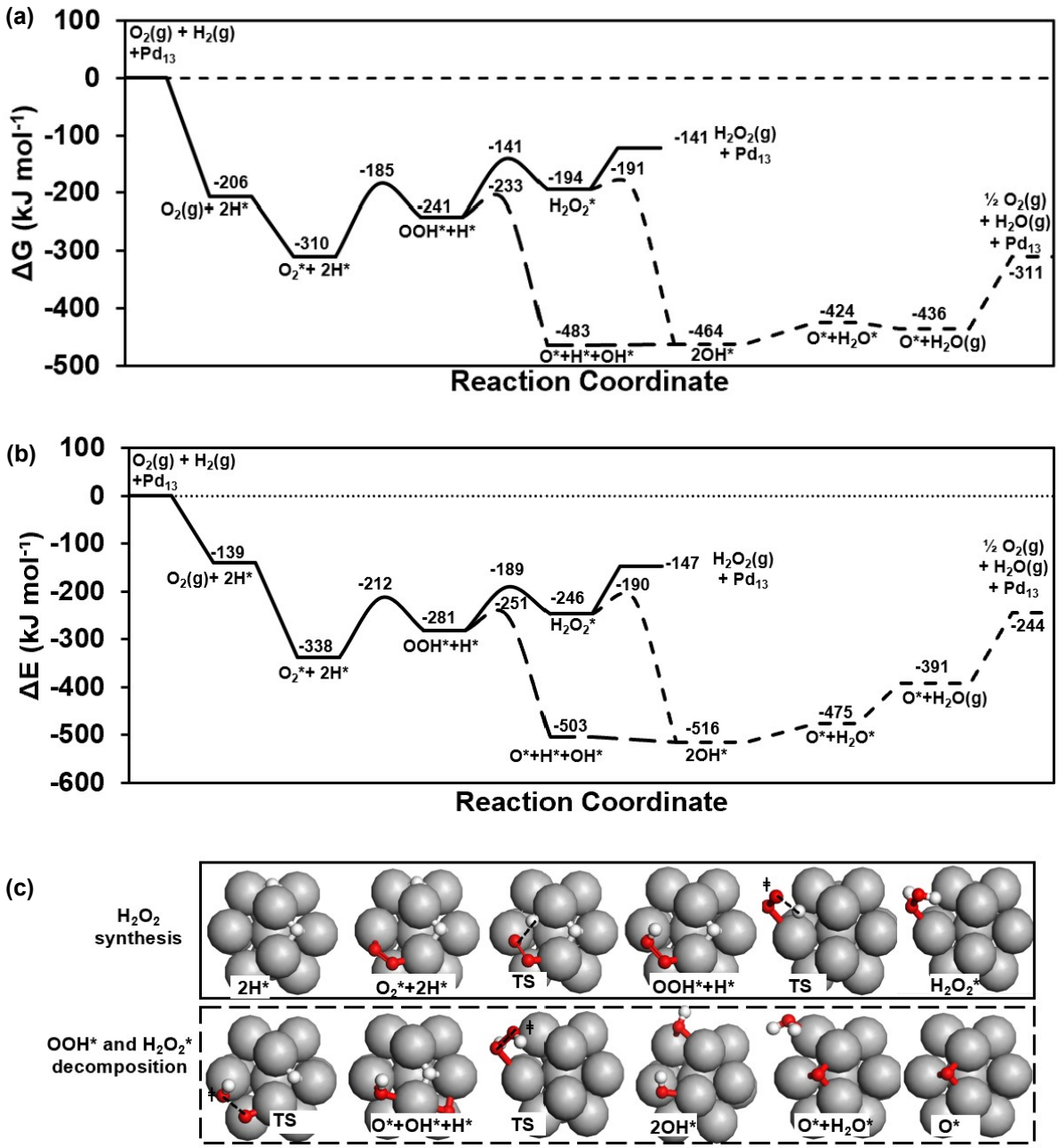

Figure S27. DFT-derived (a) Gibbs free energies, (b) electronic energies, (c) structures of intermediates and TS structures involved in the possible H_2O_2 synthesis pathways (in Scheme 1) on the Pd_{13} cluster. All energies are reference to the energies of O_2(g) and H_2(g) and the clean Pd_{13} cluster.

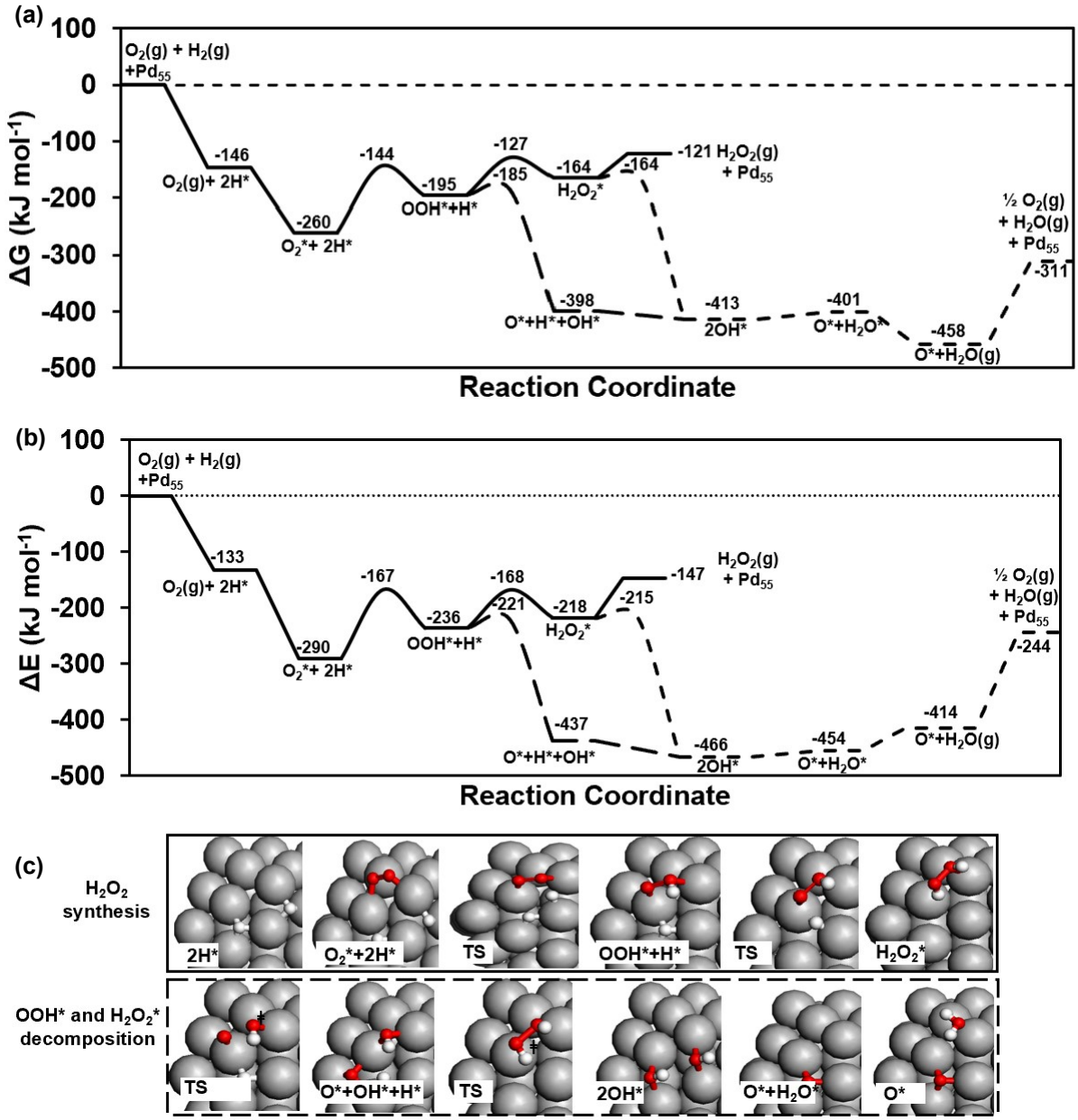

Figure S28. DFT-derived (a) Gibbs free energies, (b) electronic energies, (c) structures of intermediates and TS structures involved in the possible H_2O_2 synthesis pathways (in Scheme 1) on the Pd_{55} cluster. All energies are reference to the energies of O_2(g) and H_2(g) and the clean Pd_{55} cluster.

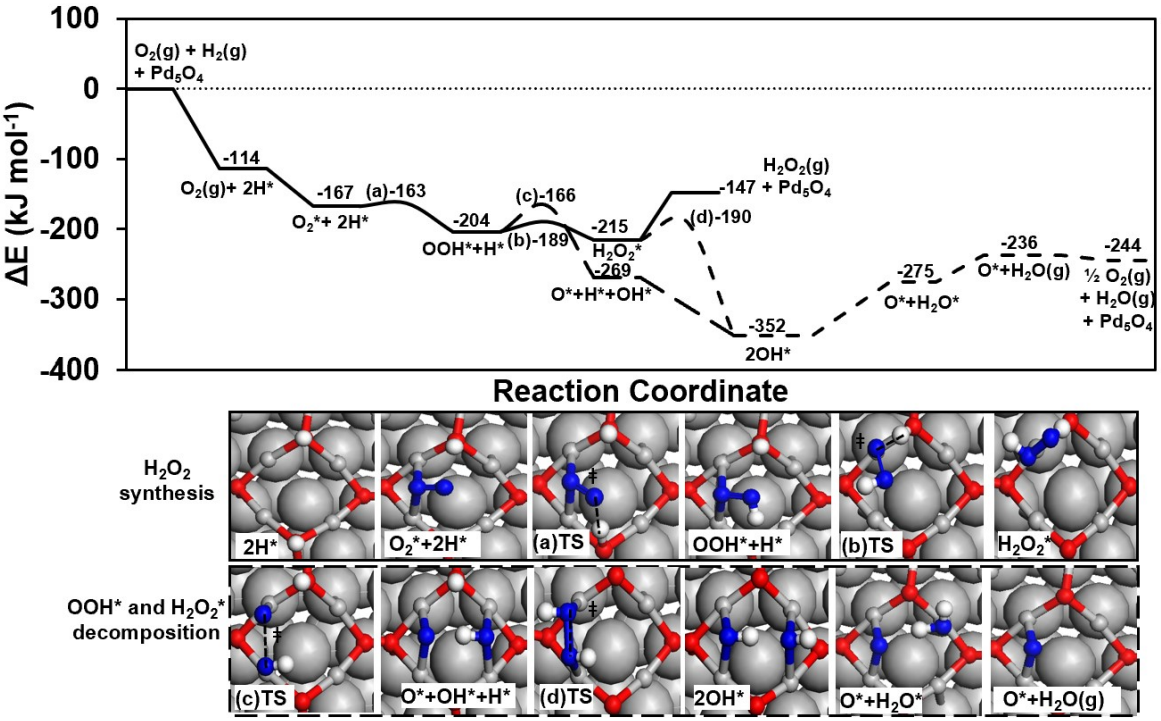

Figure S29. Electronic energies of intermediates and TS structures involved in the possible H_2O_2 synthesis pathways (in Scheme 1) on Pd_5O_4/Pd(111). All energies are referenced to the energies of O_2(g) and H_2(g) and clean Pd_5O_4/Pd(111) surface. The corresponding images on the bottom are shown for each stable species and TSs in the reaction pathway.

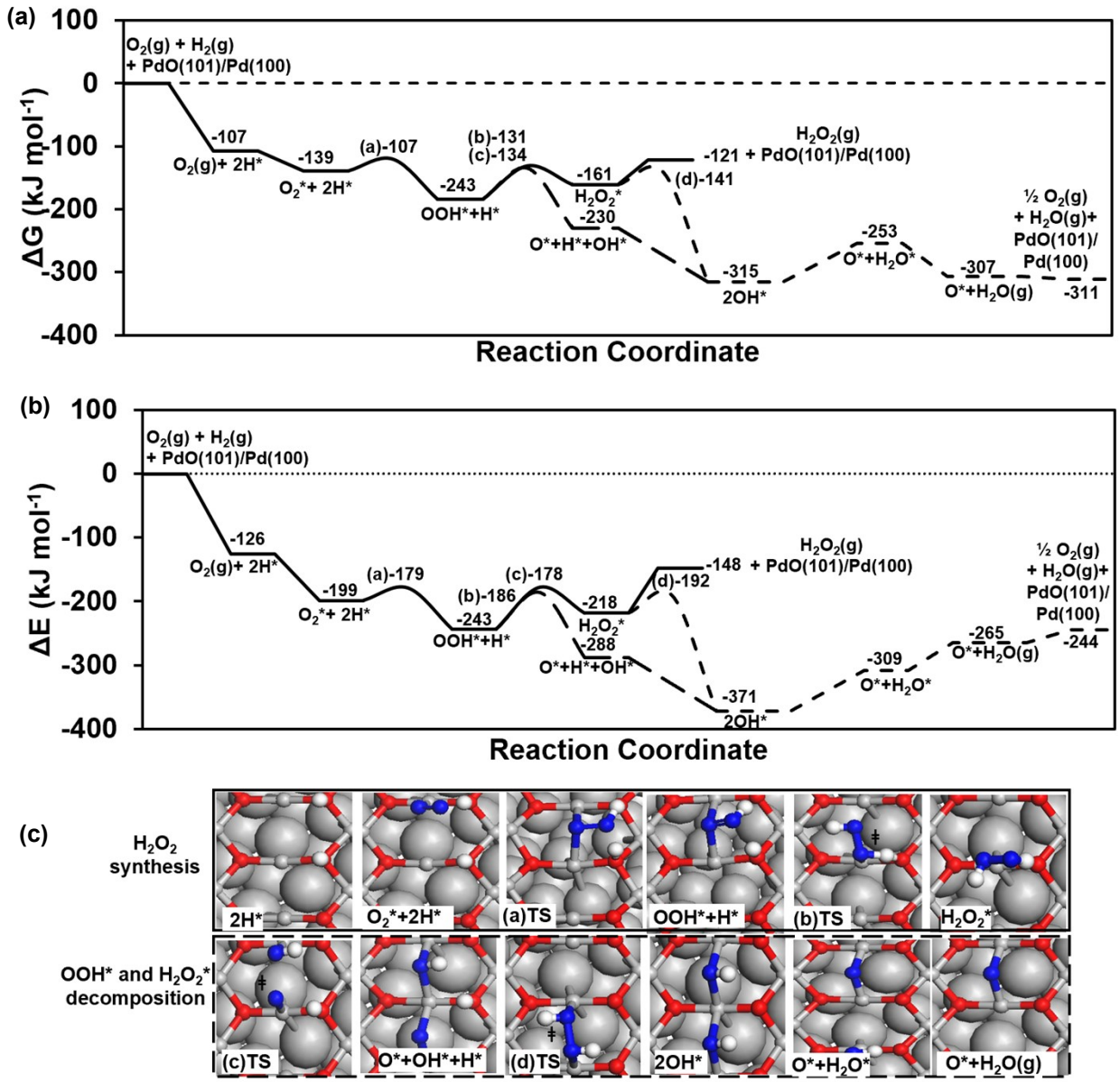

Figure S30. DFT-derived (a) Gibbs free energies, (b) electronic energies, (c) structures of intermediates and TS structures involved in the possible H_2O_2 synthesis pathways (in Scheme 1) on PdO(101)/Pd(100). All energies are reference to the energies of O_2(g) and H_2(g) and the clean PdO(101)/Pd(100) surface.

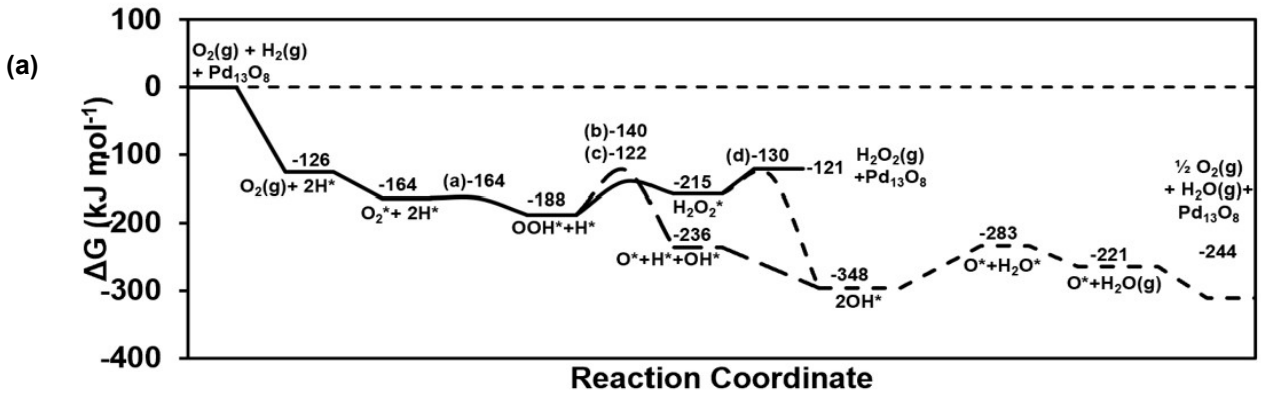

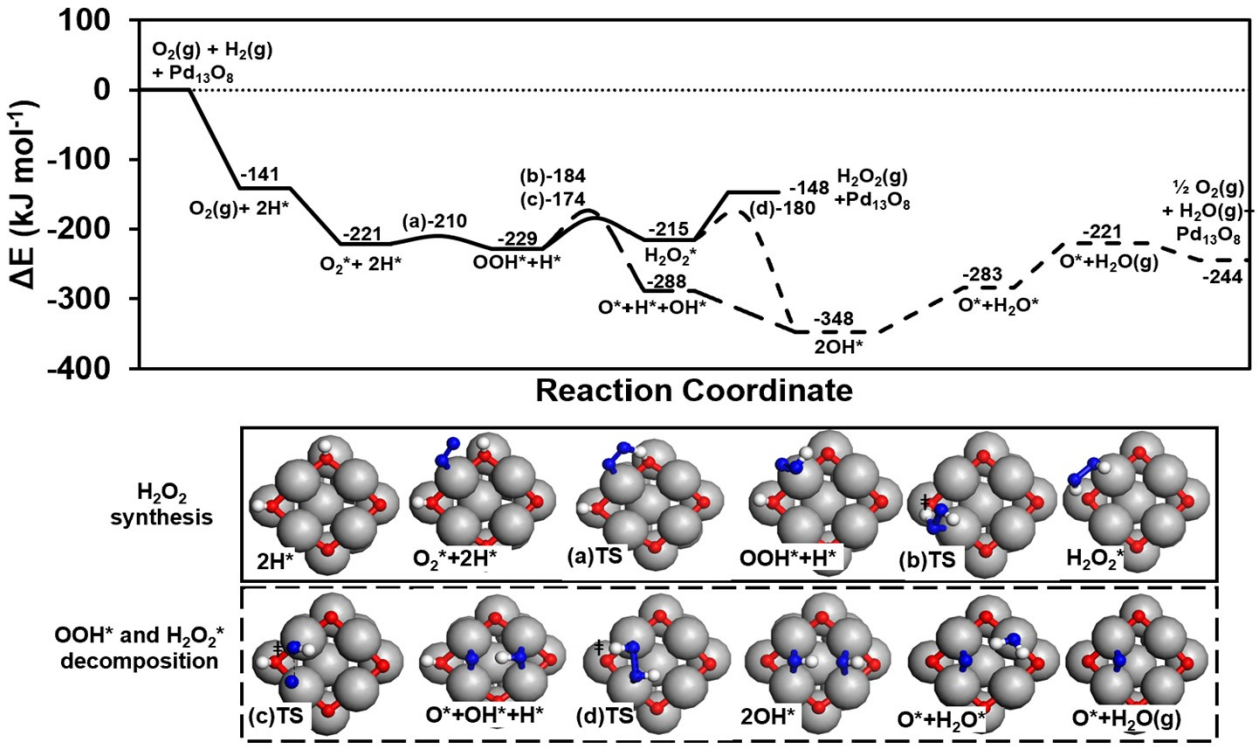

Figure S31. DFT-derived (a) Gibbs free energies, (b) electronic energies, (c) structures of intermediates and TS structures involved in the possible H_2O_2 synthesis pathways (in Scheme 1) on the $Pd_{13}O_8$ cluster. All energies are reference to the energies of O_2(g) and H_2(g) and the clean $Pd_{13}O_8$ cluster.

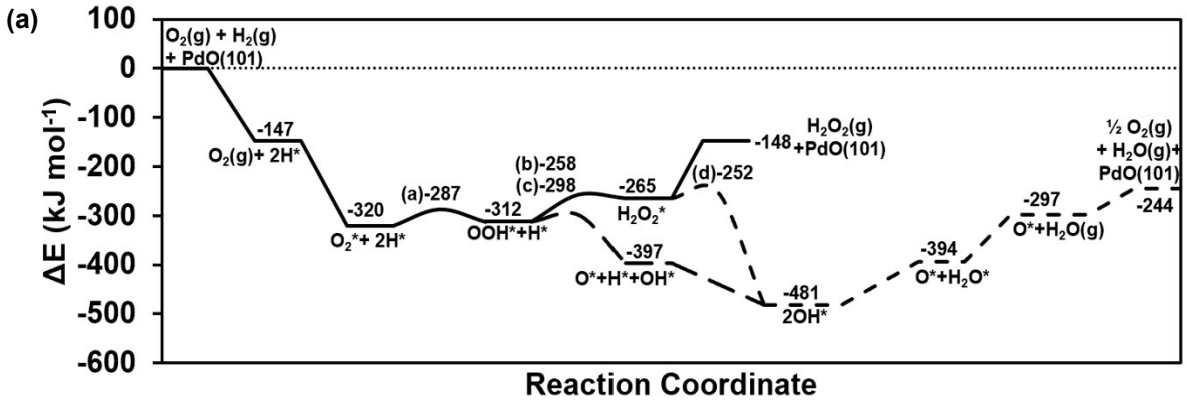

(b)

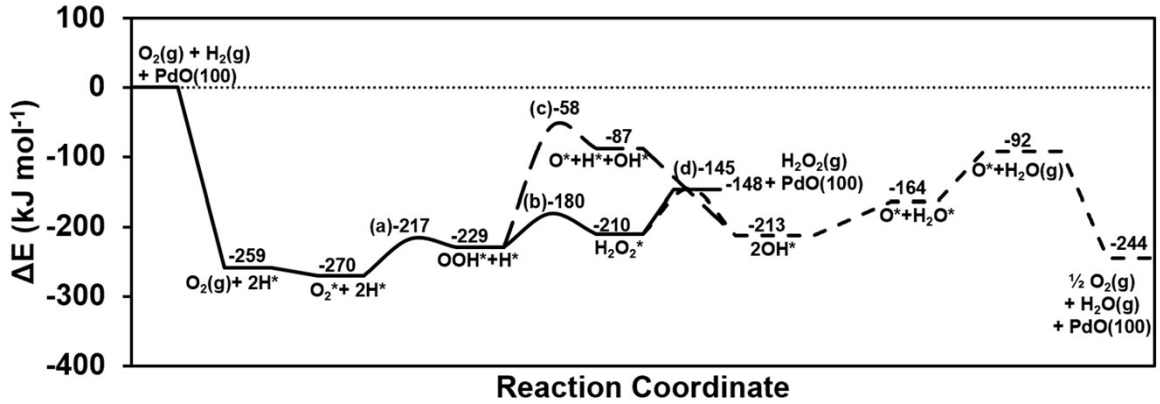

Figure S32. Electronic energies of intermediates and TS structures involved in the possible H_2O_2 synthesis pathways (in Scheme 1) on (a) PdO(100) and (b) PdO(101). All energies are referenced to the energies of O_2(g) and H_2(g) and the clean surface.

(a)

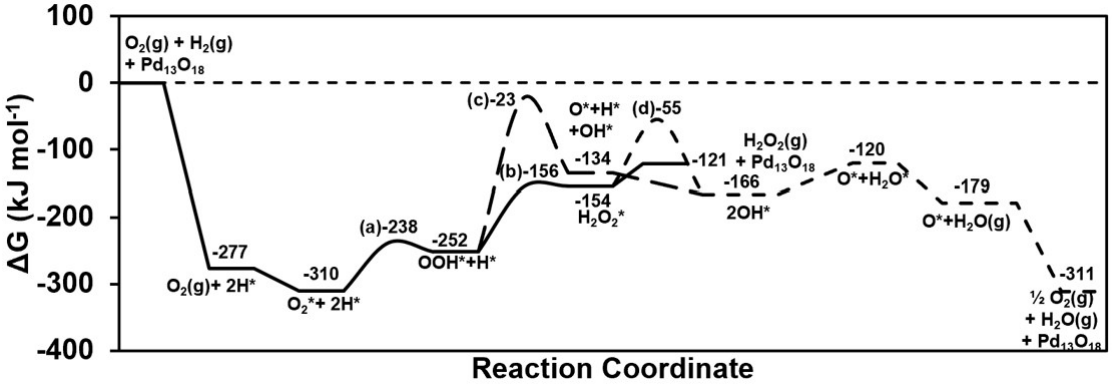

(b)

(c)

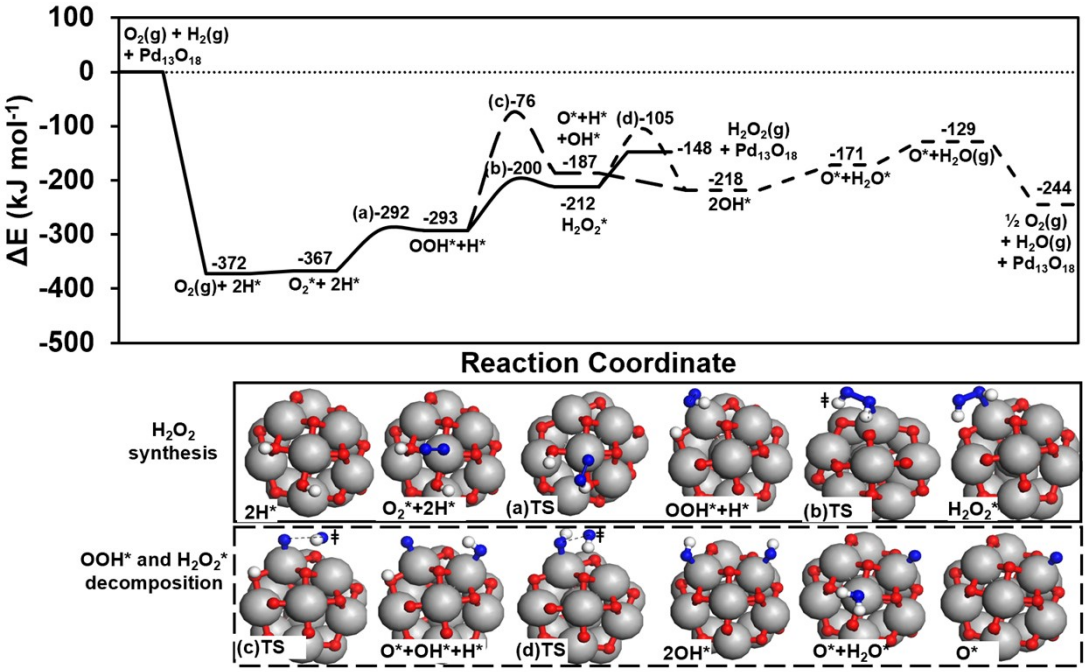

Figure S33. DFT-derived (a) Gibbs free energies, (b) electronic energies, (c) structures of intermediates and TS structures involved in the possible H_2O_2 synthesis pathways (in Scheme 1) on the $Pd_{13}O_{18}$ cluster. All energies are reference to the energies of O_2(g) and H_2(g) and the clean $Pd_{13}O_{18}$ cluster.

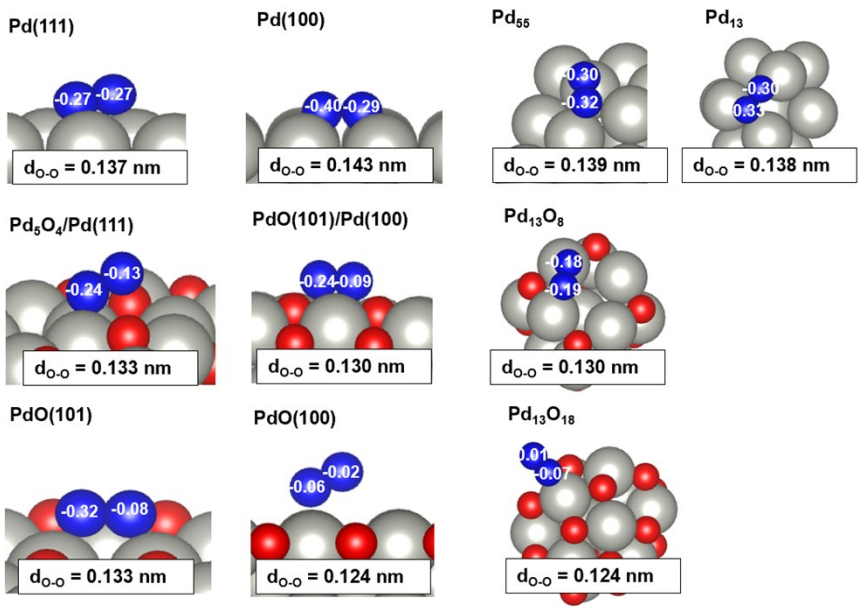

Figure S34. Charge distribution between O-atoms in surface-bound O_2* on Pd, PdO/Pd, and PdO models, obtained via Bader charge analysis. The O-O distance between O atoms in O_2* (d_{O-O}; nm) is shown.

S5. O_2 Dissociation on clean Pd surfaces

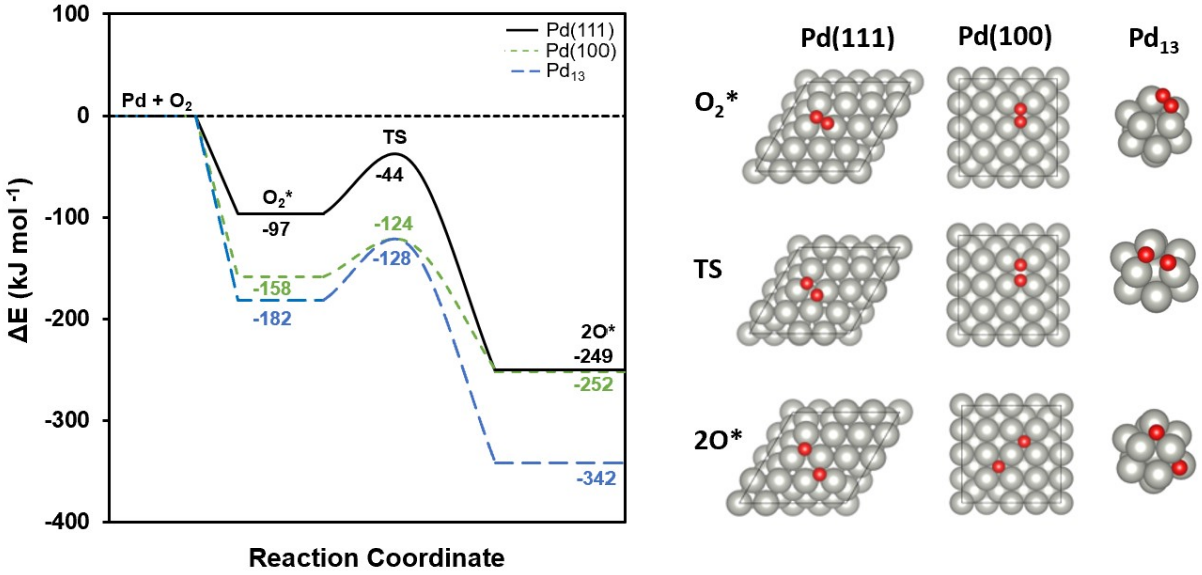

Figure S35: Electronic energies of intermediates and TS structures involved in O_2 dissociation on Pd(111), Pd(100), and Pd_{13} models. The corresponding images on the right are shown for each stable species and TS in the reaction pathway.

S6. H_2 Dissociation on Pd, PdO/Pd, and PdO surfaces

Table S12. Electronic reaction energies and activation barriers for H_2 dissociation on Pd and PdO models.

		H_2 Dissociation Reaction Energy (kJ mol^{-1})	H_2 Dissociation Activation Barrier (kJ mol^{-1})	
Metallic Pd	Pd(111)	-101	4	[12]
	Pd(100)	-78	~0	[13]
	Pd_{55}	-84	9	This work
	Pd_{13}	-73	14	This work
Bulk oxides	$Pd_{13}O_{18}$	-250	~0	This work
	PdO(101)	-145	32, 38	[14], [15]

*Reaction energies and activation barriers are reference to H_2(g) and clean Pd and PdO models. All reaction energies are from this work, while activation barriers are either from literature values or from our calculations, as noted in the table.

S7. Binding energies of O* on Pd surfaces

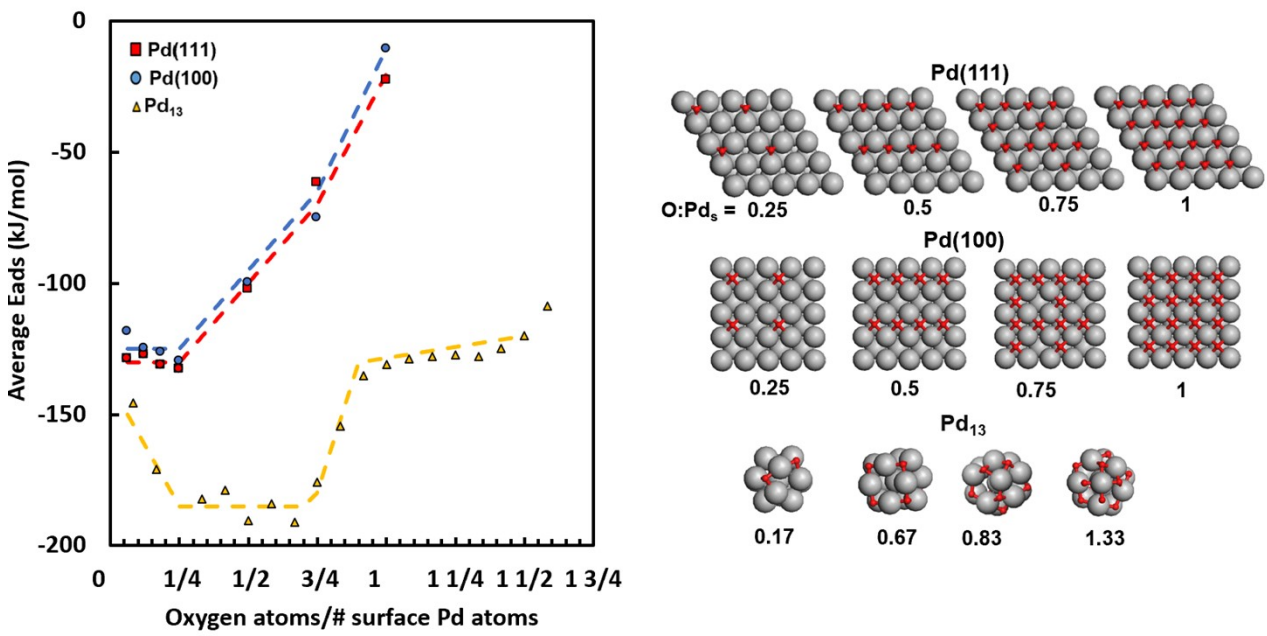

Figure S36: Average O* adsorption energies as a function of the oxygen coverage on Pd(111) (red squares), Pd(100) (blue circles), and Pd_{13} (yellow triangles). The dashed lines represent the trend in adorption energies for each model. All O* atoms bind on hollow sites in all models, and the binding configurations are shown on the right panel.

S8. Pd and PdO/Pd model structures

This section contains the VASP structure files (POSCAR/CONTCAR) for Pd and PdO/Pd models used in this work. Pd_{13}, Pd_{55}, $Pd_{13}O_8$, and $Pd_{13}O_{16}$ were obtained through DFT/MD/DFT optimization. PdO(101)/Pd(100) and Pd_5O_4/Pd(111) were created based on structural parameters found in literature and optimized with DFT, as outlined in Section 2.1 of the manuscript.

Pd_{13}

Pd13_new.cif

```
   1.00000000000000
    20.0000000000000000    0.0000000000000000    0.0000000000000000
    -0.0001000000000000   20.0000000000000000    0.0000000000000000
    -0.0001000000000000   -0.0001000000000000   20.0000000000000000
   Pd
    13
Selective dynamics
Direct
  0.5029200000000031  0.4887000000000015  0.4878300000000024   F   F   F
  0.6229736273433932  0.4882917448429289  0.4361027021495274   T   T   T
  0.6088592350060104  0.4744660174517173  0.5723463353940603   T   T   T
  0.4020137421061653  0.5077342359205029  0.3968360714472754   T   T   T
  0.3816512170387728  0.4887976009769894  0.5340843214670898   T   T   T
  0.4453377116521494  0.6051265698790759  0.4863224559380286   T   T   T
  0.5823220561736963  0.5975807092078288  0.5104216609720172   T   T   T
  0.4240290675518064  0.3803251239943553  0.4615219642360284   T   T   T
  0.5631511006429716  0.3734631480045395  0.4859403765085608   T   T   T
  0.4747405870398105  0.4030800335174761  0.5888745506195255   T   T   T
  0.4942954964312750  0.5430482231104871  0.6036993276277353   T   T   T
  0.5149545272367910  0.4331639660691007  0.3700502634407982   T   T   T
  0.5250957675948277  0.5708337278188018  0.3804753848210862   T   T   T
```

Pd_{55}

Pd55_clean.cif

1.00000000000000
30.0000000000000000 0.0000000000000000 0.0000000000000000
0.0000000000000000 31.0000000000000000 0.0000000000000000
0.0000000000000000 0.0000000000000000 32.0000000000000000
Pd
55
Selective dynamics
Direct

0.4831399999999988	0.5058300000000031	0.4905199999999965	F	F	F
0.5572562427090781	0.5058292558059099	0.4475748562143667	T	T	T
0.5572500391507255	0.5058341665326876	0.5334730807333974	T	T	T
0.4090312934865352	0.5058331425974992	0.4475582323399505	T	T	T
0.4090334931929285	0.5058345894316888	0.5334658666216204	T	T	T
0.4373114254732925	0.5775472390441497	0.4905109906067993	T	T	T
0.5289601549752084	0.5775477767816827	0.4905229803034692	T	T	T
0.4373111401407317	0.4341123489137576	0.4905123419589178	T	T	T
0.5289651351395865	0.4341035870214163	0.4905183163814337	T	T	T
0.4831380240140275	0.4614843653517699	0.5599870140480483	T	T	T
0.4831387287545489	0.5501672375646220	0.5599980875625882	T	T	T
0.4831454502171255	0.4614946488645765	0.4210448734151075	T	T	T
0.4831550284747825	0.5501637169672604	0.4210415129521463	T	T	T
0.6330996959548068	0.5058377404106055	0.4036477794315226	T	T	T
0.6348728008074139	0.5058311600668509	0.4905276032311455	T	T	T
0.6330875961562067	0.5058377715132703	0.5773960931432385	T	T	T
0.3332095215879192	0.5058354503820987	0.4036232560267231	T	T	T
0.3314203148752241	0.5058335054100407	0.4905105598498570	T	T	T
0.3331999303502436	0.5058387037278438	0.5773892530809892	T	T	T
0.3904641532211630	0.6509397355634713	0.4905136922819994	T	T	T
0.4831395670137830	0.6526604737024053	0.4905198398080033	T	T	T
0.5758178724290522	0.6509344570786233	0.4905229244202857	T	T	T
0.3904649649495118	0.3607336642696634	0.4905108212949736	T	T	T
0.4831371541502806	0.3590002972325766	0.4905204971370458	T	T	T
0.5758113708803045	0.3607280716578875	0.4905202325055587	T	T	T
0.4831436054412496	0.4161556565811955	0.6310853645897903	T	T	T
0.4831510167927373	0.5058419360605313	0.6327501913628908	T	T	T
0.4831466446044460	0.5955118542352896	0.6310777037221250	T	T	T
0.4831614041172356	0.4161534558895317	0.3499547685706907	T	T	T
0.4831665425882112	0.5058404406206364	0.3482853058413632	T	T	T
0.4831622916993782	0.5955105351163711	0.3499587992938328	T	T	T
0.5590183508208120	0.4604561736257229	0.6055970532901107	T	T	T
0.5590192994285696	0.5512096475573031	0.6055953322297344	T	T	T
0.5590280209676446	0.4604552047551331	0.3754504196056905	T	T	T
0.5590304066692386	0.5512073876903086	0.3754418963837829	T	T	T
0.4072722803885556	0.4604639338827348	0.6055935511246394	T	T	T
0.4072757189870378	0.5512113435594560	0.6056008668603257	T	T	T
0.4072816304008417	0.4604594974240971	0.3754292212966402	T	T	T
0.4072855147401538	0.5512065157856262	0.3754325453320846	T	T	T
0.6059052372512251	0.5792514234526769	0.4465687693038841	T	T	T
0.6059008151330229	0.5792511539852773	0.5344734979835146	T	T	T
0.3603880471742926	0.5792544117058925	0.4465522778772230	T	T	T
0.3603832358709819	0.5792507695583656	0.5344658840018679	T	T	T

0.6059051915553896	0.4324092345410719	0.4465710074177887	T	T	T
0.6058947583123958	0.4324039025295755	0.5344754097506617	T	T	T
0.3603905424383326	0.4324115208908403	0.4465489221645637	T	T	T
0.3603850505971809	0.4324081472701916	0.5344684493123264	T	T	T
0.4362622007658801	0.6246249394698629	0.5616357204480501	T	T	T
0.5300272272625950	0.6246281157217155	0.5616367021019186	T	T	T
0.4362529039816069	0.3870416876843359	0.5616373279119798	T	T	T
0.5300201541466628	0.3870375017029351	0.5616410711249140	T	T	T
0.4362713789912681	0.6246246034360754	0.4193946483632692	T	T	T
0.5300333624762126	0.6246299481323128	0.4194054239295518	T	T	T
0.4362626425054001	0.3870384625932317	0.4193849107718455	T	T	T
0.5300336408457610	0.3870424573061266	0.4194029903486269	T	T	T

$Pd_{13}O_8$

Pd13O8.cif

```
  1.00000000000000
   20.0000000000000000   0.0000000000000000   0.0000000000000000
   -0.0001000000000000  20.0000000000000000   0.0000000000000000
   -0.0001000000000000  -0.0001000000000000  20.0000000000000000
  O   Pd
   8   13
Selective dynamics
Direct
 0.4744035088689225  0.5105038532191405  0.3252237553137153  T  T  T
 0.6325412441358076  0.5841741835065658  0.4191950435239111  T  T  T
 0.5185512552069811  0.6424930766156350  0.5704317488998365  T  T  T
 0.3602919184878456  0.5710341320528253  0.4753365975487246  T  T  T
 0.3863211884796596  0.3949288487957965  0.5614799119018192  T  T  T
 0.5441314071329678  0.4665766973599409  0.6573415576369910  T  T  T
 0.6614932657275312  0.4096894501089875  0.5082659138424939  T  T  T
 0.5037550032691377  0.3358479555441008  0.4137564461901266  T  T  T
 0.5114999999999981  0.4925599999999974  0.4942100000000025  F  F  F
 0.6468485517682921  0.4920121362764865  0.4541315465352913  T  T  T
 0.6051580276773397  0.4369202216679775  0.5853761610407322  T  T  T
 0.4152057525944804  0.5421442692921531  0.3983501356785297  T  T  T
 0.3706936886825745  0.4852761595626269  0.5238683890963803  T  T  T
 0.4353285857635250  0.6077128543202641  0.5287569133172887  T  T  T
 0.5776204853775124  0.6166614419094190  0.4952460459754087  T  T  T
 0.4432716574682869  0.3628210556318212  0.4875080259435323  T  T  T
 0.5860801298470210  0.3745682477001645  0.4535681229051093  T  T  T
 0.4609675012814006  0.4339670198764158  0.6139010389410696  T  T  T
 0.5265884516370961  0.5562650689228720  0.6191057840984404  T  T  T
 0.4990063528618660  0.4236024283988578  0.3671000188130679  T  T  T
 0.5585456243584648  0.5414332019001858  0.3683082929067851  T  T  T
```

$Pd_{13}O_{18}$

Pd13O18.cif

1.00000000000000

20.0000000000000000 0.0000000000000000 0.0000000000000000

-0.0008000000000000 20.0000000000000000 0.0000000000000000

-0.0008000000000000 -0.0008000000000000 20.0000000000000000

O Pd

18 13

Selective dynamics

Direct

0.5951898959046230	0.3227477673474999	0.4707053437319341	T	T	T
0.5549006583632137	0.4052644205142147	0.6473071939947678	T	T	T
0.5284032604784498	0.5961675822920623	0.3759946662028336	T	T	T
0.4790770874152953	0.3506676965526571	0.5498108527930788	T	T	T
0.5756701272023441	0.5691350418292362	0.6526257961550617	T	T	T
0.4490024863465987	0.5026919024676344	0.6747897907011513	T	T	T
0.4092244294805275	0.4891541129816306	0.4195543057410352	T	T	T
0.4138357592889045	0.6283146828656875	0.4613124636044243	T	T	T
0.5030779024414486	0.3964775178793353	0.3917287137923587	T	T	T
0.6839981484298902	0.5426978621249878	0.5760874195845481	T	T	T
0.6981430046303250	0.4073895330904380	0.4310299829191762	T	T	T
0.6119641177546523	0.6459238078203816	0.4691989897499838	T	T	T
0.3874408120479306	0.4483565413823724	0.5479481167864699	T	T	T
0.6686091863398994	0.4077381037233077	0.5755471718315721	T	T	T
0.5993152480371281	0.4850535538362367	0.3521028038143240	T	T	T
0.5189839331127962	0.6568182720530238	0.5655592989183617	T	T	T
0.3877378473373371	0.5907321792600649	0.5903981744412944	T	T	T
0.7111178837255948	0.5469792575517468	0.4375010297524839	T	T	T
0.4451915622958036	0.4112187909167334	0.4746050146865912	T	T	T
0.4621880119519745	0.4293717493414259	0.6156277690698575	T	T	T
0.5030913325699515	0.4973935986993979	0.3795592541877547	T	T	T
0.3947594487838995	0.5435139567151701	0.5059491034964414	T	T	T
0.5792429268650039	0.3620534363825288	0.5558663267549552	T	T	T
0.5391800000000018	0.4992999999999981	0.5106800000000007	F	F	F
0.5082636969795153	0.6384245831607953	0.4653878735101707	T	T	T
0.6043986474946756	0.3983232180463625	0.4100554945184268	T	T	T
0.6184864149385214	0.4811637827688247	0.6229845491963221	T	T	T
0.6243112379935535	0.5689496466415254	0.4050101493083635	T	T	T
0.4774949411351045	0.5820993745686909	0.6253794299191552	T	T	T
0.6967950393854291	0.4742416144950615	0.5002338095887151	T	T	T
0.6061527739972945	0.6070096417650462	0.5632230349054245	T	T	T

PdO(101)/Pd(100)

PdO101Pd100.cif
1.00000000000000
12.3550000000000004 0.0000000000000000 0.0000000000000000
0.0000000000000000 12.3550000000000004 0.0000000000000000
-0.0004000000000000 -0.0004000000000000 20.8604999999999983
O Pd
16 96
Selective dynamics
Direct

0.3545586954339991	0.4196300022975722	0.3756205275645035	T	T	T
0.1604423396562572	0.4222640917093195	0.4302506492724312	T	T	T
0.3585586910176949	0.1734735862668336	0.3778695688433899	T	T	T
0.1636599769369194	0.1704941851301769	0.4323404310876384	T	T	T
0.8545586920014329	0.4196299994515644	0.3756205171832165	T	T	T
0.6604423558625943	0.4222640966570255	0.4302506511125002	T	T	T
0.8585587102248398	0.1734735992420615	0.3778695630519006	T	T	T
0.6636599763900612	0.1704941976352755	0.4323404365252514	T	T	T
0.3545587026604954	0.9196299840154065	0.3756205070484546	T	T	T
0.1604423185642872	0.9222640906346894	0.4302506514310792	T	T	T
0.3585587195850996	0.6734735744122058	0.3778695410093918	T	T	T
0.1636599633734626	0.6704941732412228	0.4323404274848018	T	T	T
0.8545587172645756	0.9196299814966539	0.3756205189883006	T	T	T
0.6604423046510394	0.9222640785867139	0.4302506572157354	T	T	T
0.8585587150633412	0.6734735640034796	0.3778695630366453	T	T	T
0.6636599741446528	0.6704941666788145	0.4323404267487546	T	T	T
0.0000000000000000	0.0000000000000000	0.0936499999999967	F	F	F
0.1000000000000014	0.2999999999999972	0.0936499999999967	F	F	F
0.3999999999999986	0.2000000000000028	0.0936499999999967	F	F	F
0.0006700529520544	0.0075910749102284	0.2803809717419430	T	T	T
0.0980155250532368	0.3051699556963914	0.2876298076872452	T	T	T
0.3979596540914507	0.2019082391189506	0.2826734164712718	T	T	T
0.2000000000000028	0.1000000000000014	0.0936499999999967	F	F	F
0.2999999999999972	0.3999999999999986	0.0936499999999967	F	F	F
0.1913931555269519	0.1047504054564762	0.2826536987094543	T	T	T
0.2990320760123364	0.4054410103697350	0.2814998721131244	T	T	T
0.0499999999999972	0.1499999999999986	0.0000000000000000	F	F	F
0.1499999999999986	0.4500000000000028	0.0000000000000000	F	F	F
0.3500000000000014	0.0499999999999972	0.0000000000000000	F	F	F
0.4500000000000028	0.3500000000000014	0.0000000000000000	F	F	F
0.0486199999999997	0.1522500000000022	0.1865299999999976	F	F	F
0.1497600000000006	0.4495599999999982	0.1876499999999979	F	F	F
0.3477099999999993	0.0518700000000010	0.1861699999999971	F	F	F
0.4508599999999987	0.3503400000000028	0.1878799999999998	F	F	F
0.2500000000000000	0.2500000000000000	0.0000000000000000	F	F	F
0.2482699999999980	0.2524500000000032	0.1880299999999977	F	F	F
0.0133065208580427	0.4186332114125148	0.3951788861461673	T	T	T
0.2582241691858507	0.0469117186183146	0.4031968176214019	T	T	T
0.0164145684638106	0.1718756866789344	0.3980474147866350	T	T	T
0.2563632171734041	0.2960679254345268	0.4040377054588384	T	T	T
0.5000000000000000	0.0000000000000000	0.0936499999999967	F	F	F
0.6000000000000014	0.2999999999999972	0.0936499999999967	F	F	F

0.8999999999999986	0.2000000000000028	0.0936499999999967	F	F	F
0.5006700385241952	0.0075910561329224	0.2803809758528253	T	T	T
0.5980155312315699	0.3051699610824398	0.2876298167576976	T	T	T
0.8979596593351955	0.2019082482656453	0.2826734171342418	T	T	T
0.7000000000000028	0.1000000000000014	0.0936499999999967	F	F	F
0.7999999999999972	0.3999999999999986	0.0936499999999967	F	F	F
0.6913931695897854	0.1047504083747009	0.2826537010041703	T	T	T
0.7990320942394388	0.4054410056210779	0.2814998831745955	T	T	T
0.5499999999999972	0.1499999999999986	0.0000000000000000	F	F	F
0.6499999999999986	0.4500000000000028	0.0000000000000000	F	F	F
0.8500000000000014	0.0499999999999972	0.0000000000000000	F	F	F
0.9500000000000028	0.3500000000000014	0.0000000000000000	F	F	F
0.5486199999999997	0.1522500000000022	0.1865299999999976	F	F	F
0.6497600000000006	0.4495599999999982	0.1876499999999979	F	F	F
0.8477099999999993	0.0518700000000010	0.1861699999999971	F	F	F
0.9508599999999987	0.3503400000000028	0.1878799999999998	F	F	F
0.7500000000000000	0.2500000000000000	0.0000000000000000	F	F	F
0.7482699999999980	0.2524500000000032	0.1880299999999977	F	F	F
0.5133065363997619	0.4186332120905454	0.3951788905904057	T	T	T
0.7582241822084681	0.0469117075027946	0.4031968283293756	T	T	T
0.5164145565056319	0.1718756835324221	0.3980474155903843	T	T	T
0.7563632154706039	0.2960679486579208	0.4040377023066462	T	T	T
0.0000000000000000	0.5000000000000000	0.0936499999999967	F	F	F
0.1000000000000014	0.7999999999999972	0.0936499999999967	F	F	F
0.3999999999999986	0.7000000000000028	0.0936499999999967	F	F	F
0.0006700582900498	0.5075910757314070	0.2803809696824778	T	T	T
0.0980155317488155	0.8051699584378635	0.2876298066923162	T	T	T
0.3979596417573459	0.7019082433737882	0.2826734382828687	T	T	T
0.2000000000000028	0.6000000000000014	0.0936499999999967	F	F	F
0.2999999999999972	0.8999999999999986	0.0936499999999967	F	F	F
0.1913931583286156	0.6047504125522917	0.2826537020104733	T	T	T
0.2990320931844115	0.9054409971009277	0.2814998856614570	T	T	T
0.0499999999999972	0.6499999999999986	0.0000000000000000	F	F	F
0.1499999999999986	0.9500000000000028	0.0000000000000000	F	F	F
0.3500000000000014	0.5499999999999972	0.0000000000000000	F	F	F
0.4500000000000028	0.8500000000000014	0.0000000000000000	F	F	F
0.0486199999999997	0.6522500000000022	0.1865299999999976	F	F	F
0.1497600000000006	0.9495599999999982	0.1876499999999979	F	F	F
0.3477099999999993	0.5518700000000010	0.1861699999999971	F	F	F
0.4508599999999987	0.8503400000000028	0.1878799999999998	F	F	F
0.2500000000000000	0.7500000000000000	0.0000000000000000	F	F	F
0.2482699999999980	0.7524500000000032	0.1880299999999977	F	F	F
0.0133065489224670	0.9186332102826040	0.3951788835357513	T	T	T
0.2582241800338580	0.5469117329688141	0.4031968140994222	T	T	T
0.0164145627217113	0.6718756911177010	0.3980474106405156	T	T	T
0.2563632177547879	0.7960679391740131	0.4040377037576492	T	T	T
0.5000000000000000	0.5000000000000000	0.0936499999999967	F	F	F
0.6000000000000014	0.7999999999999972	0.0936499999999967	F	F	F
0.8999999999999986	0.7000000000000028	0.0936499999999967	F	F	F
0.5006700475884610	0.5075910810565635	0.2803809738262941	T	T	T
0.5980155214885047	0.8051699591091440	0.2876298065529033	T	T	T

0.8979596545727097	0.7019082366316279	0.2826734288510149	T	T	T
0.7000000000000028	0.6000000000000014	0.0936499999999967	F	F	F
0.7999999999999972	0.8999999999999986	0.0936499999999967	F	F	F
0.6913931590384310	0.6047504134643136	0.2826537050376809	T	T	T
0.7990320817449169	0.9054410027763894	0.2814998743606256	T	T	T
0.5499999999999972	0.6499999999999986	0.0000000000000000	F	F	F
0.6499999999999986	0.9500000000000028	0.0000000000000000	F	F	F
0.8500000000000014	0.5499999999999972	0.0000000000000000	F	F	F
0.9500000000000028	0.8500000000000014	0.0000000000000000	F	F	F
0.5486199999999997	0.6522500000000022	0.1865299999999976	F	F	F
0.6497600000000006	0.9495599999999982	0.1876499999999979	F	F	F
0.8477099999999993	0.5518700000000010	0.1861699999999971	F	F	F
0.9508599999999987	0.8503400000000028	0.1878799999999998	F	F	F
0.7500000000000000	0.7500000000000000	0.0000000000000000	F	F	F
0.7482699999999980	0.7524500000000032	0.1880299999999977	F	F	F
0.5133065495293624	0.9186332070206554	0.3951788838756740	T	T	T
0.7582241716502393	0.5469117171870099	0.4031968120422710	T	T	T
0.5164145555416982	0.6718756908713736	0.3980474096493727	T	T	T
0.7563632161581446	0.7960679389619291	0.4040377054084138	T	T	T

Pd_5O_4/Pd(111)

Pd5O4
1.00000000000000
11.0507000000000009 0.0000000000000000 0.0000000000000000
-16.5761000234783928 28.7104000406654194 0.0000000000000000
0.0000000000000000 -0.0001378226773401 19.9999999995251230
O Pd
28 179
Selective dynamics
Direct

0.5670166252873852	0.0866060489346731	0.3844681880859424	T	T	T
0.6337271692720181	0.2160426130858512	0.3360176370459177	T	T	T
0.3862689573977899	0.1218147178570053	0.3764367652432187	T	T	T
0.7982675599775183	0.1760901650670553	0.3337622333429890	T	T	T
0.4009983690259473	0.2694476101529333	0.3930648021676737	T	T	T
0.6828653835651813	0.3933842526971623	0.3287156794959580	T	T	T
0.9184369834058391	0.3428296785324423	0.3976919485210442	T	T	T
0.7180519269378014	0.5139388833034108	0.3823481574993414	T	T	T
0.5017085543554486	0.5730491861895064	0.3323261201934773	T	T	T
0.8629589414863127	0.6865858412135919	0.3790417605107675	T	T	T
0.4656414063113964	0.4213027145051891	0.3360294468053742	T	T	T
0.8987336792175808	0.4848435536176421	0.3307590796767861	T	T	T
0.1532533405426199	0.2945955525049919	0.3797001155561786	T	T	T
0.3454342912066006	0.6171174532718130	0.3872344256851256	T	T	T
0.1660044050252427	0.6560918677887199	0.3348392145772617	T	T	T
0.4638668241943485	0.7847805233859156	0.3821239726785653	T	T	T
0.6953544261064661	0.7303370829751619	0.3800711616583216	T	T	T
0.4622171661918571	0.9044625816098573	0.3846214795918640	T	T	T
0.2733160663208041	0.8184797464273564	0.3919632128296677	T	T	T
0.7003003983506166	0.8774353096143315	0.3754777433975777	T	T	T
0.0169202822869172	0.0080118359606107	0.3362802793091447	T	T	T
0.9410900022971738	0.8206362494763931	0.3327139979053202	T	T	T
0.2419832553165021	0.4819663730563690	0.3804356103648970	T	T	T
0.1235311030530569	0.5351942090196320	0.4041981290297646	T	T	T
0.1528060597582550	0.1775520269912386	0.3778639091772654	T	T	T
0.2397438308439118	0.9653086452404896	0.3359757115255349	T	T	T
0.7657071306285397	0.0204215203528516	0.3205749520495252	T	T	T
0.8812054136327613	0.0969147579738523	0.3828301117325928	T	T	T
0.9847608689833792	0.9886568195947486	0.2339437918645126	T	T	T
0.1527020791419271	0.0199633928539160	0.1160143156518520	T	T	T
0.0833299999999966	0.0555599999213072	0.0000000000000000	F	F	F
0.2250824483687523	0.9831025910171348	0.2379685303290862	T	T	T
0.3996029178025939	0.0197190931279727	0.1173923860854308	T	T	T
0.3333299999999966	0.0555599999213072	0.0000000000000000	F	F	F
0.4834884999466606	0.9882448621305313	0.2321388543909744	T	T	T
0.6505354463161733	0.0209954496274598	0.1131888324064984	T	T	T
0.5833299999999966	0.0555599999213072	0.0000000000000000	F	F	F
0.7369838165460622	0.9905167133272489	0.2260192547720316	T	T	T
0.9043789486742236	0.0216948277288371	0.1135776672195042	T	T	T
0.8333299999999966	0.0555599999213072	0.0000000000000000	F	F	F
0.9910496992706103	0.0745768977327275	0.2253973085601162	T	T	T
0.1582759356534472	0.1052536341749815	0.1140646979031810	T	T	T

0.0833299999999966	0.1388899998032826	0.0000000000000000	F	F	F
0.2339637194041261	0.0712492026098991	0.2258974439963474	T	T	T
0.4057176378652967	0.1040177914212336	0.1137717217554484	T	T	T
0.3333299999999966	0.1388899998032826	0.0000000000000000	F	F	F
0.4802440510765326	0.0712580738469201	0.2307995300625400	T	T	T
0.6525505656370617	0.1050656696342134	0.1157501571090286	T	T	T
0.5833299999999966	0.1388899998032826	0.0000000000000000	F	F	F
0.7356575694197561	0.0748319347743601	0.2229932968577044	T	T	T
0.9062303806257991	0.1050975136012436	0.1127868390824003	T	T	T
0.8333299999999966	0.1388899998032826	0.0000000000000000	F	F	F
0.9853817495332363	0.1560037431614201	0.2272477255442080	T	T	T
0.1577607192608417	0.1888477206487847	0.1160070953395185	T	T	T
0.0833299999999966	0.2222199996852510	0.0000000000000000	F	F	F
0.2291832364763091	0.1547291224346348	0.2314834579094282	T	T	T
0.4061951022984045	0.1882080730763313	0.1151467272659736	T	T	T
0.3333299999999966	0.2222199996852510	0.0000000000000000	F	F	F
0.4732931320435520	0.1529868913657966	0.2293859063985177	T	T	T
0.6537164434610871	0.1879637450964911	0.1159237737881166	T	T	T
0.5833299999999966	0.2222199996852510	0.0000000000000000	F	F	F
0.7377566182789731	0.1562765892220641	0.2314338098556734	T	T	T
0.9051014037762068	0.1882014323100629	0.1131996592234172	T	T	T
0.8333299999999966	0.2222199996852510	0.0000000000000000	F	F	F
0.9786309903991024	0.2386411660606175	0.2246133845355794	T	T	T
0.1550692855559397	0.2721333167440021	0.1147084313809116	T	T	T
0.0833299999999966	0.3055599995672011	0.0000000000000000	F	F	F
0.2226174629829061	0.2377947349315641	0.2339313580882574	T	T	T
0.4024047886851551	0.2715338438436881	0.1151268722730203	T	T	T
0.3333299999999966	0.3055599995672011	0.0000000000000000	F	F	F
0.4661103475104431	0.2368417620066213	0.2298251606704752	T	T	T
0.6516545459080115	0.2713042193469877	0.1176020019925428	T	T	T
0.5833299999999966	0.3055599995672011	0.0000000000000000	F	F	F
0.7161077330281320	0.2352541894071418	0.2345773060530257	T	T	T
0.8983467177398580	0.2710645037184379	0.1173065502876126	T	T	T
0.8333299999999966	0.3055599995672011	0.0000000000000000	F	F	F
0.9667857933838009	0.3195862830337777	0.2346728145461821	T	T	T
0.1469373833926750	0.3539746969404850	0.1160331910075256	T	T	T
0.0833299999999966	0.3888899994491766	0.0000000000000000	F	F	F
0.2165353698582776	0.3207338006110204	0.2313483397148326	T	T	T
0.4006251086739488	0.3552373880606840	0.1174330011247355	T	T	T
0.3333299999999966	0.3888899994491766	0.0000000000000000	F	F	F
0.4620397195761403	0.3192253967180010	0.2303935979761160	T	T	T
0.6493962907032074	0.3535374318846287	0.1141251086917742	T	T	T
0.5833299999999966	0.3888899994491766	0.0000000000000000	F	F	F
0.7147321167171273	0.3184368737774568	0.2370515647526712	T	T	T
0.8983253525083142	0.3540219809798808	0.1179049412596054	T	T	T
0.8333299999999966	0.3888899994491766	0.0000000000000000	F	F	F
0.9626938744658113	0.4041889310480343	0.2332935496035981	T	T	T
0.1458308915101564	0.4377194278064899	0.1157952042683557	T	T	T
0.0833299999999966	0.4722199993311449	0.0000000000000000	F	F	F
0.2181710000386810	0.4059610425394818	0.2276298879521291	T	T	T
0.3968133043929447	0.4380909264669293	0.1142785924422997	T	T	T

0.3333299999999966	0.4722199993311449	0.0000000000000000	F	F	F
0.4632287956182479	0.4057147071943549	0.2318677643397938	T	T	T
0.6468730004670600	0.4376715436209931	0.1147937477526493	T	T	T
0.5833299999999966	0.4722199993311449	0.0000000000000000	F	F	F
0.7077277966989457	0.4015418869506770	0.2260763509806500	T	T	T
0.8963170949094083	0.4368932644020249	0.1167147422042378	T	T	T
0.8333299999999966	0.4722199993311449	0.0000000000000000	F	F	F
0.9442242995086119	0.4872288538443371	0.2325506110957933	T	T	T
0.1415073248811346	0.5204100576208242	0.1190072810103983	T	T	T
0.0833299999999966	0.5555599992131022	0.0000000000000000	F	F	F
0.2067570024253900	0.4872429771818582	0.2338439509369939	T	T	T
0.3908946025584076	0.5214420607399605	0.1157854085427512	T	T	T
0.3333299999999966	0.5555599992131022	0.0000000000000000	F	F	F
0.4610792477338719	0.4901262129684542	0.2277025395575989	T	T	T
0.6426587566256734	0.5218046387882666	0.1145148047854980	T	T	T
0.5833299999999966	0.5555599992131022	0.0000000000000000	F	F	F
0.7042553589329748	0.4905303753175166	0.2260208325262565	T	T	T
0.8938186404018675	0.5204450820932542	0.1139720624011421	T	T	T
0.8333299999999966	0.5555599992131022	0.0000000000000000	F	F	F
0.9568939929551220	0.5715363988525682	0.2273808790387913	T	T	T
0.1419432764350105	0.6035890103953128	0.1173200292663635	T	T	T
0.0833299999999966	0.6388899990950776	0.0000000000000000	F	F	F
0.2016515075998930	0.5691265575325631	0.2364791221597899	T	T	T
0.3903293424855436	0.6042623520193242	0.1185224693054829	T	T	T
0.3333299999999966	0.6388899990950776	0.0000000000000000	F	F	F
0.4569177861528716	0.5720236276313342	0.2313512301075094	T	T	T
0.6418789308027759	0.6049109410208717	0.1145869453819253	T	T	T
0.5833299999999966	0.6388899990950776	0.0000000000000000	F	F	F
0.7109013464374727	0.5740534006076260	0.2292477511782223	T	T	T
0.8917419503874855	0.6042581275744343	0.1142735380264627	T	T	T
0.8333299999999966	0.6388899990950776	0.0000000000000000	F	F	F
0.9544614612385950	0.6547341790282242	0.2270569980432140	T	T	T
0.1419718153690167	0.6870533604020397	0.1134030667057258	T	T	T
0.0833299999999966	0.7222199989770459	0.0000000000000000	F	F	F
0.2002977930233417	0.6529938593809017	0.2322689499783459	T	T	T
0.3899922138426990	0.6873715836799372	0.1175597879384668	T	T	T
0.3333299999999966	0.7222199989770459	0.0000000000000000	F	F	F
0.4520180581161674	0.6528404015656459	0.2351007554179960	T	T	T
0.6395163965462624	0.6877142038963170	0.1153665247893702	T	T	T
0.5833299999999966	0.7222199989770459	0.0000000000000000	F	F	F
0.7073398920143156	0.6566718637724267	0.2285174902146800	T	T	T
0.8913447696364012	0.6876786216862193	0.1139736723705091	T	T	T
0.8333299999999966	0.7222199989770459	0.0000000000000000	F	F	F
0.9622925145243231	0.7378589803463489	0.2285074437289106	T	T	T
0.1420800724780857	0.7707590331202286	0.1148389367562173	T	T	T
0.0833299999999966	0.8055599988590032	0.0000000000000000	F	F	F
0.2125228151614820	0.7367806049616346	0.2252685989974335	T	T	T
0.3949006662525897	0.7712182244999567	0.1171938053288151	T	T	T
0.3333299999999966	0.8055599988590032	0.0000000000000000	F	F	F
0.4598857452437162	0.7356291091174929	0.2354891940987462	T	T	T
0.6405198141519267	0.7708418638090323	0.1165526407919477	T	T	T

0.5833299999999966	0.8055599988590032	0.0000000000000000	F	F	F
0.7062400577172222	0.7368264648004296	0.2317904247570819	T	T	T
0.8896527506249976	0.7706431296469276	0.1154774123739844	T	T	T
0.8333299999999966	0.8055599988590032	0.0000000000000000	F	F	F
0.9577369095876086	0.8201947037685158	0.2294233491238648	T	T	T
0.1422606998059051	0.8534242516924999	0.1157668423540517	T	T	T
0.0833299999999966	0.8888899987409786	0.0000000000000000	F	F	F
0.2138549187461138	0.8198360587358943	0.2320194544815400	T	T	T
0.3932084854281477	0.8536022050883010	0.1177798466972761	T	T	T
0.3333299999999966	0.8888899987409786	0.0000000000000000	F	F	F
0.4603921928393687	0.8184489951667987	0.2375407764207325	T	T	T
0.6426587417367099	0.8544303023943516	0.1174858212366356	T	T	T
0.5833299999999966	0.8888899987409786	0.0000000000000000	F	F	F
0.7069830766551294	0.8191546619454245	0.2313532085287660	T	T	T
0.8921392670011673	0.8545586101707676	0.1159893801290697	T	T	T
0.8333299999999966	0.8888899987409786	0.0000000000000000	F	F	F
0.9655223636156735	0.9029717878967258	0.2350665838357242	T	T	T
0.1449748105854348	0.9366269073541375	0.1177799611538126	T	T	T
0.0833299999999966	0.9722199986229469	0.0000000000000000	F	F	F
0.2188196564370855	0.9010055359218715	0.2303159551096235	T	T	T
0.3966293749025743	0.9367985591905930	0.1167852611380726	T	T	T
0.3333299999999966	0.9722199986229469	0.0000000000000000	F	F	F
0.4698668023394370	0.9027658150873130	0.2328975171219958	T	T	T
0.6467402230506947	0.9377473428313596	0.1177726944710210	T	T	T
0.5833299999999966	0.9722199986229469	0.0000000000000000	F	F	F
0.7143347583884089	0.9026272057734389	0.2334590172432672	T	T	T
0.8967389083984729	0.9381617835046950	0.1200249286882819	T	T	T
0.8333299999999966	0.9722199986229469	0.0000000000000000	F	F	F
0.5923054906118160	0.1484466302802901	0.3562471347665159	T	T	T
0.4976497274564018	0.2378049613477867	0.3573064298409713	T	T	T
0.5226562806983366	0.3320482393017595	0.3569619382877612	T	T	T
0.7898228555345363	0.2802179304693035	0.3637532463927359	T	T	T
0.8210851628024621	0.3733430028931462	0.3584242363563335	T	T	T
0.1953605317721968	0.2429233275590078	0.3654553617797143	T	T	T
0.6919231546089049	0.4540712559467934	0.3487405272154733	T	T	T
0.5908630787566755	0.5347973442072314	0.3512854604316639	T	T	T
0.6833325654122032	0.6327370905264458	0.3529020250588616	T	T	T
0.8711490108334319	0.5756691137120883	0.3468067650842503	T	T	T
0.0058824580422922	0.6692227971387541	0.3533840826837870	T	T	T
0.3070135254953996	0.3555272518375392	0.3528997216156002	T	T	T
0.1344986091750278	0.5922711248324130	0.3615940364003297	T	T	T
0.3186105839634835	0.7218458505784192	0.3549508250968495	T	T	T
0.5204019163875175	0.6715463397981730	0.3622125711541226	T	T	T
0.6021507257569765	0.7661966387165424	0.3659435178229207	T	T	T
0.4755705357122331	0.8464386933005978	0.3682669922334864	T	T	T
0.1568985757294576	0.7606886683559632	0.3400382598076994	T	T	T
0.1388584775476055	0.8371518381035701	0.3601978160402770	T	T	T
0.3389547831763438	0.9291178300908408	0.3507375590609930	T	T	T
0.6254728004455814	0.9595475703646872	0.3535355109118798	T	T	T
0.8443012262381695	0.9418987428670840	0.3529026325787182	T	T	T
0.8931427707039143	0.7504624590495290	0.3516711836849597	T	T	T

0.8161179793538190	0.8491644456741895	0.3514601179622129	T	T	T
0.3138886583573748	0.5524476169592969	0.3735080904429235	T	T	T
0.0863488342101715	0.3755652753787988	0.3398520249054682	T	T	T
0.3518197235914913	0.4536979768741931	0.3499930580582279	T	T	T
0.2737713055789250	0.1521472009147584	0.3590735057410078	T	T	T
0.2235087987782301	0.0603486630827909	0.3531083501611915	T	T	T
0.4017308888304791	0.0274474691026459	0.3546258105274678	T	T	T
0.6776101472388439	0.0592855351743349	0.3496827945648612	T	T	T
0.9597639244268090	0.2452999474330537	0.3506353710611390	T	T	T
0.9598444324614100	0.1627154774652308	0.3545885656463957	T	T	T
0.9705795819240004	0.0586923839617408	0.3544904025957027	T	T	T
0.0466508913491636	0.4706892756542791	0.3555053672466668	T	T	T

References

(1) Doye, J. P. K.; Wales, D. J. Global Minima for Transition Metal Clusters Described by Sutton–Chen Potentials. New Journal of Chemistry 1998, 22 (7), 733–744. https://doi.org/10.1039/A709249K.
(2) Rapps, T.; Ahlrichs, R.; Waldt, E.; Kappes, M. M.; Schooss, D.; Rapps, T.; Ahlrichs, R.; Waldt, E.; Kappes, M. M.; Schooss, D. On the Structures of 55-Atom Transition-Metal Clusters and Their Relationship to the Crystalline Bulk. Angewandte Chemie International Edition 2013, 52 (23), 6102–6105. https://doi.org/10.1002/ANIE.201302165.
(3) Xing, X.; Hermann, A.; Kuang, X.; Ju, M.; Lu, C.; Jin, Y.; Xia, X.; Maroulis, G. Insights into the Geometries, Electronic and Magnetic Properties of Neutral and Charged Palladium Clusters. Scientific Reports 2016, 6 (1), 1–11. https://doi.org/10.1038/srep19656.
(4) Nava, P.; Sierka, M..; Ahlrichs, R. Density Functional Study of Palladium Clusters. Physical Chemistry Chemical Physics 2003, 34 (43). https://doi.org/10.1039/B303347C
(5) Reuter, K.; Scheffler, M. Composition and Structure of the RuO_2 110 Surface in an O_2 and CO Environment: Implications for the Catalytic Formation of CO_2. https://doi.org/10.1103/PhysRevB.68.045407.
(6) Rogal, J.; Reuter K. Ab Initio Atomistic Thermodynamics for Surfaces: A Primer. 2007.
(7) Plauck, A.; Stangland, E. E.; Dumesic, J. A.; Mavrikakis, M. Active Sites and Mechanisms for H_2O_2 Decomposition over Pd Catalysts. Proc Natl Acad Sci U S A 2016, 113 (14), E1973–E1982. https://doi.org/10.1073/pnas.1602172113.
(8) McQuarrie, D. A. Statistical Mechanics. 2000, 641.
(9) Flaherty, D. W. Direct Synthesis of H_2O_2 from H_2 and O_2 on Pd Catalysts: Current Understanding, Outstanding Questions, and Research Needs. ACS Catal 2018, 8 (2), 1520–1527. https://doi.org/10.1021/acscatal.7b04107
(10) Bravo-Suárez, J. J.; Bando, K. K.; Akita, T.; Fujitani, T.; Fuhrer, T. J.; Oyama, S. T. Propane Reacts with O_2 and H_2 on Gold Supported TS-1 to Form Oxygenates with High Selectivity. *Chemical Communications* 2008, No. 28, 3272–3274. https://doi.org/10.1039/B800620B.
(11) Campbell, C. T.; Selers, J. R. V. The Entropies of Adsorbed Molecules. J Am Chem Soc 2012, 134 (43), 18109–18115. https://doi.org/10.1021/ja3080117
(12) Li, J.; Ishihara, T.; Yoshizawa, K. Theoretical Revisit of the Direct Synthesis of H_2O_2 on Pd and Au@Pd Surfaces: A Comprehensive Mechanistic Study. Journal of Physical Chemistry C 2011, 115 (51), 25359–25367. https://doi.org/10.1021/jp208118e
(13) Tian, P.; Ouyang, L.; Xu, X; Han, Y. F. Density functional theory study of direct synthesis of H_2O_2 from H_2 and O_2 on Pd(111), Pd(100), and Pd(110) surfaces. Chinese Journal of Catalysis. 2013, 34 (5), 1002-1012.. https://doi.org/10.1016/S1872-2067(12)60537-3
(14) Martin, N. M.; Van Den Bossche, M.; Grönbeck, H.; Hakanoglu, C.; Gustafson, J.; Blomberg, S.; Arman, M. A.; Antony, A.; Rai, R.; Asthagiri, A.; Weaver, J. F.; Lundgren, E. Dissociative Adsorption of Hydrogen on PdO(101) Studied by HRCLS and DFT. Journal of Physical Chemistry C 2013, 117 (26), 13510–13519. https://doi.org/10.1021/jp4036698
(15) Sun, X.; Peng, X.; Xu, X.; Jin, H.; Wang, H.; Wang, X. H_2 Adsorption and Dissociation on PdO(101) Films Supported on Rutile TiO_2 (110) Facet: Elucidating the Support Effect by DFT Calculations. J Mol Model 2016, 22 (9), 1–8. https://doi.prg/10.1007/s00894-016-3072-3